Nonlinear detection of third harmonic generation (THG) in gold metamaterial

by

Onwukwe .Barth. Ikenna
B.Sc., Crawford University, Nigeria, 2010.

A Project Report Submitted in Partial Fulfillment
of the Requirements for the Degree of

MASTER OF ENGINEERING

in the Department of Electrical and Computer Engineering

Supervisory Committee

Nonlinear detection of third harmonic generation (THG) in gold metamaterial

by

Onwukwe .Barth. Ikenna
B.Sc., Crawford University, Nigeria, 2010.

Supervisory Committee

Dr. Reuven Gordon, Supervisor
(Department of Electrical and Computer Engineering)

Dr. Thomas .E. Darcie, Member
(Department of Electrical and Computer Engineering)

Abstract

Supervisory Committee
Dr. Reuven Gordon, Supervisor
(Department of Electrical and Computer Engineering)

Dr. Thomas .E. Darcie, Member
(Department of Electrical and Computer Engineering)

This report investigates the optical nonlinearity in thin gold film metasurfaces with an aperture array to realize third harmonic generation (THG). Using Lumerical finite difference time domain (FDTD), nonlinear third harmonic generation was simulated and compared to previous reported works on nonlinear scattering theory. The proposed FDTD nonlinear simulation is computational friendly, simple and provides a good case study when considering the effect of higher excitation power on metamaterials to realise THG, as compared to past simulations carried out that involves importing data from Lumerical FDTD to Matlab to carry out the nonlinear scattering calculation to obtain the final result. The conversion efficiency (the ratio of THG power to the excitation power) of three different aperture arrays was obtained with results showing that the H-shape array would give the highest conversion efficiency of about 0.52 %. The result shows that the FDTD nonlinear simulation approach used agrees with the experimental result and nonlinear scattering theory. This project points towards an effective detection of third harmonic generation (THG) from thin plasmonic metal films using the finite difference time domain (FDTD) method.

Table of Contents

List of Tables

List of Figures

Acknowledgments

I would like to thank GOD and my parents for providing for me all through my education.

I would also like to thank

Dr. Reuven Gordon for guiding me through graduate studies and all the students of the nanoplasmonics Research Lab for their support and knowledge.

Chapter 1: Introduction

Nonlinear optics is a branch of optics that describes the change of a materials optical property in the presence of an intense light [1]. This field of research is growing for all photonics technologies, with many recent published papers and conferences about nonlinear optics. The recent interest can be said to be stimulated by the applications of optics in areas such as telecommunication, information processing and medicine. In order to observe non-linear effect in metamaterials, one would require a light source that is sufficiently intense to change the optical properties of the metamaterial and make the optical properties of the metamaterial system depend on the intensity of the light.

Nonlinear optics is utilized in nonlinear optical devices and techniques that are important in many applications to engineers and science researchers. Some of these applications are all optical switching, wavelength conversion, and near-field imaging [2-7]. The origin of nonlinear optics can be traced to the discovery of second harmonic generation by Peter Franken et al. in 1961 [8].

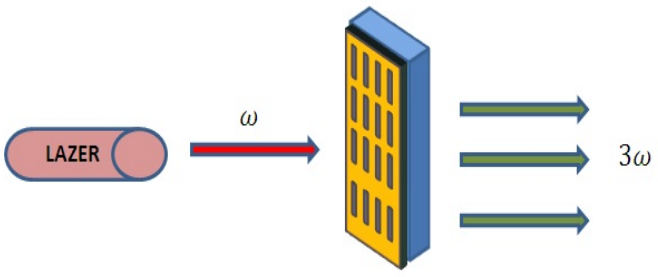

Figure 1.1: Diagram of Third Harmonic Generation (THG) in a rectangular aperture metamaterial.

This breakthrough led to the study of the behaviour of materials that exhibit nonlinearity [9]. Previously, researchers considered harmonic generation based on the material system and design, with many suggesting that metamaterials are better for the detection of harmonic generation [2]. Metamaterials have been used by researches as a building block because of their plasmonic resonance that can be regulated and the fact that their linear optical properties are known [10-12].

Various studies have looked into the nonlinearity in metasurfaces based on second harmonic generation (SHG) using different apertures and shapes [13-19]. A few works have shown that aperture-structures are effective for regulating the temperature of the metal structure to yield better conversion efficiency [20-22]. Note that finding a nonlinear optical material with a large third-order nonlinear optical susceptibility has always been a challenge [1, 23].

This project involves a finite difference time domain (FDTD) simulation, using a nonlinear gold film material that is tuned to its third order nonlinear susceptibility. The design schematic used was selected because of its various advantages; starting from the effective conversion efficiency of an aperture based array to the cubic dependence of third harmonic generation to give higher conversion efficiency. The proposed nonlinear FDTD simulation measures the propagating nonlinear susceptibility that originates from the metals free electrons in the aperture array of the gold film. This simulation can be used to further justify and regulate the nonlinearity in metasurfaces for a better efficiency in some application of optics such as wavelength conversion. The main goal of this project is to show that the finite difference time domain (FDTD) nonlinear simulation agrees with the experimental result and nonlinear scattering theory. The nonlinear

scattering theory that uses a linear FDTD simulation is faster than the FDTD nonlinear scattering simulation due to the complex nature of nonlinear simulations in Lumerical FDTD as compared to the linear simulation. However, the FDTD nonlinear scattering simulation is better than the linear FDTD simulation in terms of computation and generation of final results. With the FDTD nonlinear scattering simulation, users get their final results at the end of the simulation unlike the linear FDTD simulation that would require one to import all data into Matlab to carry out the nonlinear scattering theory computation. Note that one can simulate with higher powers in a nonlinear FDTD simulation unlike the linear FDTD simulation.

The simulation agrees with the theory of nonlinear scattering, with results showing that the H-shape aperture is the best shape for producing the highest conversion efficiency using a gap size of 30 nm, a third order nonlinear susceptibility of 7.71 $\times 10^{-19}\ m^2/V^2$ and a fixed periodicity between apertures of 528 nm.

1.1 Report Structure

The rest of this report is organized as follows: Chapter 2 gives a brief review of the background to nonlinear optics. Chapter 3 describes the theoretical models in nonlinear optics that were used in the simulation and in chapter 4, an introduction to Lumerical software, simulation set-up and the results from the simulation was discussed. Chapter 5 gives a summary of the work done and proposed future works to be carried out.

Chapter 2: Background Study

Nonlinear optics started with the discovery of laser in 1960 by Maiman [24]. Miaman showed that the response of atoms to an intense electromagnetic field is no longer linear. Shortly after Miamans discovery, Franken and his group carried out an experiment that gave birth to the first nonlinear harmonic effect ever observer in 1961 [8]. Franken's experiment showed the first harmonic generation, now known to be second harmonic generation (SHG). He increased the spectral power of a ruby laser beam (to 6942 Å), and propagated the laser beam through the crystal quartz to observe an ultraviolet radiation of 3471 Å. From 1961 to 1964, various nonlinear optical phenomena were discovered with many research groups showing interest and exploring various ways of explaining and enhancing the nonlinear optical phenomena. Some of the nonlinear optical effects processes discovered during this period are four wave mixing, stimulated Raman scattering, intensity dependent refractive index and stimulated Brillouin scattering [25-30]. Many have found the field of nonlinear optics to be fascinating and some people have tried to explain the theory behind nonlinear optics. Presently, the three known textbooks in nonlinear optics are:

[1]. Y. R. Shen, The Principles of Nonlinear Optics (John Wiley and Sons, 2002).

[2]. P. N. Butcher and D. Cotter, The Elements of Nonlinear Optics (Cambridge University Press Revised edition, 1991).

[3]. R. W. Boyd, Nonlinear Optics (Academic Press, Third Edition 2008).

All three books have different views of some nonlinear phenomena, but they all agreed that the observation of a nonlinear optical effect would require a laser. A laser is the only

light source capable of providing sufficient optical intensity to activate observable nonlinear optical process.

In 1966, Yee's scheme [31], now known as finite-difference time-domain (FDTD) by Taflove in 1980 [32], introduced a numerical way to solve the differential equations that can be used to solve Maxwell's equations. Over the years many researches have explored optical phenomena based on enhanced four wave mixing [33], second harmonic generation (SHG) from metamaterials [34-36], plasmon enhanced generation of high harmonics [37-38] and third order nonlinearity. In the early years of nonlinear optics, most research groups made use of crystal to generate harmonics. Metamaterials were used to replace crystal because of the advantage of its metasuface to enhance optical nonlinearities at plasmonic resonances by some order of magnitude.

Metamaterials are artificial structures engineered to have optical properties that are not found in nature. These optical properties can be a single or multi-layered nano- metallic objects that are fabricated on the surface of a standard material. An interesting subset of metamaterials with a reduced dimensionality that demonstrates an exceptional ability for controlling the flow of light is known as metasurface [10]. These can be used to enhance nonlinear optical properties too. To date, more research works are carried out on SHG as compared to THG in the field of nonlinear optics. Different groups have looked into SHG based on material structure and metal thin film [18, 39].

Boyd et al. discussed the importance of the value of third order nonlinear optical susceptibility for metamaterials and he reported some values of third order nonlinear optical susceptibility that various research group got from experiments [40]. Over the years, research works pointed out the effect of metasurface on the second harmonic signal

generated and saw that they were able to control the signal generated from the nonlinear metamaterial using the metasurface [41-45]. Gold is used as a metamaterial because of its high plasmonics effect.

Third harmonic generation (THG) is becoming an interesting subject to researchers in optics with various research groups starting to explore and publish papers on THG in the recent years than never before [46-47]. My group recently looked into various ways of enhancing third harmonic generation that produced two papers. Ghazal et al. [48] explored the inter-band transition resonance of a gold nanoparticle on a metal film with a thin gap to measure an enhanced third harmonic generation. Not to long after her experiment, Nezami et al. [49] also investigated the effect of localized surface plasmons propagating through an aperture, based on the detection of third harmonic generation. Nezami's experiment reported a high conversion efficiency of about 0.05 %.

Melentie et al. [22, 50] was the first, to the best of my knowledge, to report the use of aluminum as a metamaterial to be the best element for observing a strong optical nonlinearity. His work showed that aluminum can give a better strong optical nonlinearity than gold, hence a better conversion efficiency. For the sake of this simulation, gold was used as a metamaterial instead of aluminium.

Chapter 3: Nonlinear Optical Theory

3.1 Introduction

The nonlinear theory used in this simulation could be compared to the experiment carried out by Nezami et al. [49]. The theory uses Lorentz reciprocity [51-52] to predict the nonlinear optical response of a metamaterial, and it was recently reported to be very efficient [39, 42]. In linear optics, the relationship between the polarization and the electric field strength is represented by;

$$\widetilde{\boldsymbol{P}}(\boldsymbol{t}) = \boldsymbol{\varepsilon_o}\boldsymbol{\chi}^{(1)}\widetilde{\boldsymbol{E}}(\boldsymbol{t}) \tag{3.1}$$

But in general, the optical response of a nonlinear phenomenon is generalized as a Taylor series in terms of the polarization and field strength.

$$\widetilde{\boldsymbol{P}}(\boldsymbol{t}) = \boldsymbol{\varepsilon_o}\left[\boldsymbol{\chi}^{(1)}\widetilde{\boldsymbol{E}}(\boldsymbol{t}) + \boldsymbol{\chi}^{(2)}\widetilde{\boldsymbol{E}}^{\boldsymbol{2}}(\boldsymbol{t}) + \boldsymbol{\chi}^{(3)}\widetilde{\boldsymbol{E}}^{\boldsymbol{3}}(\boldsymbol{t}) + \cdots\right] \tag{3.2}$$

Where $\tilde{P}(t)$ is the induced polarization, $\tilde{E}(t)$ is the electric field strength and $\chi^{(1)}$, $\chi^{(2)}$ and $\chi^{(3)}$ are known as the linear, second and third order nonlinear optical susceptibilities respectively [1].

The rest of this chapter reviews the basic theoretical models in a nonlinear optical process, such as nonlinear wave equation, THG, nonlinear scattering theory and the nonlinear optical response of metasurface based on palsmonics.

3.2 Wave Equation for Nonlinear Optical Material

In this section, we would review the basic wave equation for electromagnetic waves to find the harmonic and fundamental wavelength of the electric fields that was applied in

this project. The derivation of a classical nonlinear wave equation in a nonlinear optical media starts from Maxwell's equations [53].

$$\nabla . \mathbf{D} = \boldsymbol{\rho_{ext}} \quad \text{(Gauss' Law)} \tag{3.3}$$

$$\nabla . \mathbf{B} = \mathbf{0} \quad \text{(Gauss' Magnetism Law)} \tag{3.4}$$

$$\nabla \times \mathbf{E} = -\frac{\partial \mathbf{B}}{\partial \mathbf{t}} \quad \text{(Faraday's Law)} \tag{3.5}$$

$$\nabla \times \mathbf{H} = \frac{\partial \mathbf{D}}{\partial \mathbf{t}} + \mathbf{J} \quad \text{(Ampere's Law)} \tag{3.6}$$

Where D is the dielectric displacement, B is the magnetic induction, $\boldsymbol{\rho_{ext}}$ is the electric charge density and J is the current charge density.

In nonlinear optics, the polarization field (P) is given in terms of linear and nonlinear fields. Moreover, it is assumed that we are working in a region of space where no free charges are present and there is no magnetization in the medium. This is used to derive the wave equation in a nonlinear material in terms of electric field and nonlinear polarization density as shown in equation (3.8) [1].

$$\boldsymbol{P} = \boldsymbol{P_L} + \boldsymbol{P_{NL}} \tag{3.7}$$

$$-\nabla^2 \boldsymbol{E} + \frac{\boldsymbol{\epsilon^{(1)}}}{\boldsymbol{c^2}} \frac{\boldsymbol{\partial^2 \widetilde{E}}}{\boldsymbol{\partial t^2}} = -\frac{\mathbf{1}}{\boldsymbol{\varepsilon_o c^2}} \frac{\boldsymbol{\partial^2 \widetilde{P}_{NL}}}{\boldsymbol{\partial t^2}} \tag{3.8}$$

For free waves propagating with a velocity (c/n), the linear refractive index is proportional to the scalar quantity $\boldsymbol{\epsilon^{(1)}}$such that:

$$n^2 = \boldsymbol{\epsilon^{(1)}} \tag{3.9}$$

3.3 Third Harmonic Generation

The theory behind third harmonic generation (THG) is simple. It involves the destruction of three photons of frequency (ω) to produce a single photon with three times the

frequency in each quantum mechanical process [1]. THG occurs when the free electrons in the surface of a metamaterial are excited by an electromagnetic field, causing them to oscillate in their ionic core resulting to a nonlinear displacement that is acted upon by a returning force that gives rise to an anharmonic response in the motion of the electron with respect to the electric field applied. The complete oscillation of the electron from its equilibrium position near the surface of the nano-structure produces THG [54].

There are various applications of third harmonic generation, one of which includes optical image processing [55] that is used in the field of biology to create third harmonic microscope.

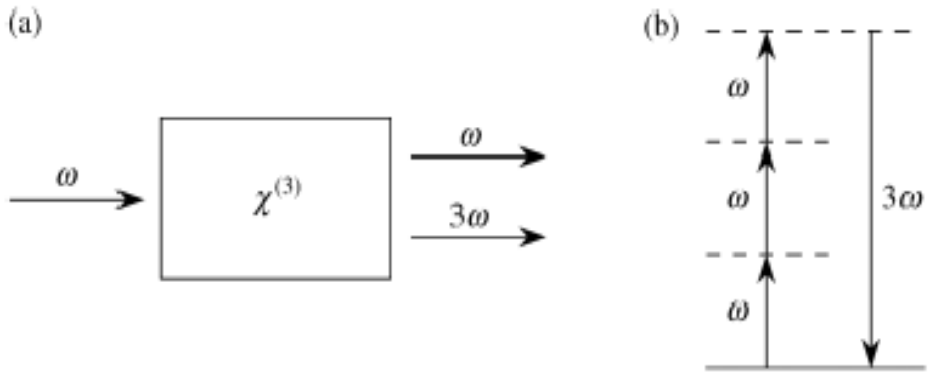

Figure 3.1: (a) Third harmonic generation process. (b) energy-level description of THG. Reprinted with permission from Ref. [1]

Fig (3.1) shows the generation of third order nonlinear optical process, with the energy level diagram showing how many photons of frequency (ω) is required to create the parametric process known as third harmonic generation [1]. One should note that for any metamaterial, the nonlinear susceptibility "$\boldsymbol{\chi}^{(3)}$" of the material is an important property that is responsible for all the nonlinear processes occurring in a medium and the nonlinear

response of the medium. Equation (3.9) shows the nonlinear polarization equation for a third order nonlinear optical polarized material.

$$\widetilde{\boldsymbol{P}}^{(3)}(\boldsymbol{t}) = \boldsymbol{\varepsilon_o}\boldsymbol{\chi}^{(3)}\widetilde{\boldsymbol{E}}^{3}(\boldsymbol{t}) \tag{3.10}$$

Where $\widetilde{\boldsymbol{P}}^{(3)}$ is the third order polarization, $\boldsymbol{\chi}^{(3)}$ is the third order nonlinear susceptibility and $\boldsymbol{\varepsilon_o}$ is the permittivity of free space.

In general third order nonlinear polarization is responsible for four wave mixing (FWM), that involves mixing three photons of frequency ω_1, ω_2 and ω_3 to generate a forth photon field with frequency $\omega_{FWM} = \omega_1 \pm \omega_2 \pm \omega_3$. From the theory of third harmonic generation, there are sixteen possible mixing processes that can be observed [1]. Third harmonic generation is the case where the harmonic is three times the fundamental frequency.

3.4 Phase Matching

Phase matching is a collection of techniques that is used to enhance the amplitude of a polarized wave radiating from a nonlinear medium. It involves matching the phase of a fundamental beam with the harmonic wave propagating through a medium to allow constructive interference. This can be aided by using a periodic structure. Hence, phase matching helps to achieve an optimum nonlinear frequency conversion between interacting waves in the direction of propagation.

3.5 Nonlinear Scattering Theory

Based on past works on nonlinear optical effects, the nonlinear scattering theory presented by O'Brien et al. [39], was found to be efficient in predicting the nonlinear optical response of a U-shaped particle under-going a SHG process as shown in fig. (3.2).

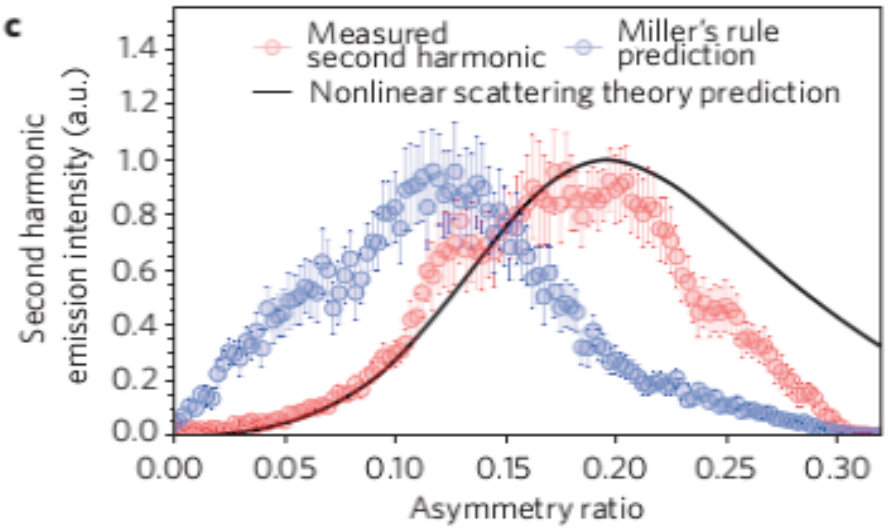

Figure 3.2: Plot showing the comparison between Miller's rule and nonlinear scattering theory to the measure SHG value. Reprinted with permission from Ref. [39]

His nonlinear scattering theory as shown in fig. (3.3) involves the use of Lorentz reciprocity theorem to model the integral relation between localized sources and their corresponding electric field in a reciprocal medium, such that two current sources $\boldsymbol{j_1}(r,\omega)$ and $\boldsymbol{j_2}(r,\omega)$ with a corresponding electric field of $\boldsymbol{E_1}(r,\omega)$ and $\boldsymbol{E_2}(r,\omega)$ in a reciprocal medium are given by:

$$\int \boldsymbol{j_2}(r',\omega)\cdot\boldsymbol{E_1}(r',\omega)\,dV' = \int \boldsymbol{j_1}(r,\omega)\cdot\boldsymbol{E_2}(r,\omega)\,dV \tag{3.11}$$

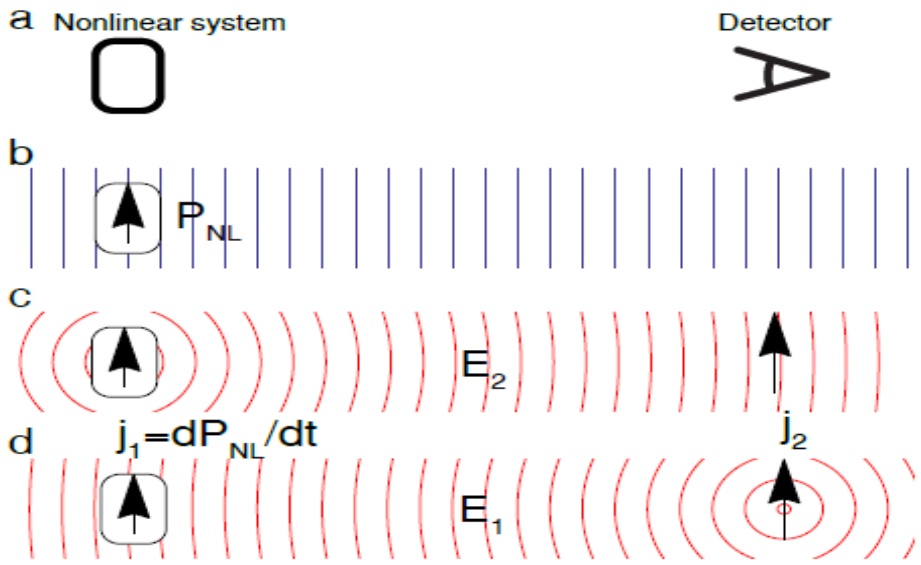

Figure 3.3: Illustration of nonlinear scattering theory showing the use of a nonlinear optical material and a detector to calculate the nonlinear emission at the detector when the nonlinear system is excited by a pump field. Reprinted with permission from Ref. [39]

The derivation further goes to show that for a nonlinear dipole on the surface or volume of a nanostructure influenced by the selection of a single source to act as the stimulating factor, can be used to calculate the nonlinear emission for the current source selected as shown in equation (3.12) assuming current source $\boldsymbol{j_1}(r,\omega)$ was selected:

$$\mathbf{E_1}\cdot\hat{\jmath} = \frac{e^{-i\omega t}}{J_0\Delta l}\int i\omega\mathbf{P}\cdot\boldsymbol{E_2}dV \tag{3.12}$$

Where $\hat{\jmath}$ is the polarization axis of the current dipole of the second current source, Δl is the length between the unknown electric field $\mathbf{E_1}$ and the emitted electric field $\boldsymbol{E_2}(r,\omega)$.

$$J = \frac{dP}{dt} \tag{3.13}$$

$$J_{3\omega} = i\omega P^{(3)} \tag{3.14}$$

O'Brien's derivation of nonlinear scattering theory was mirrored by Nezami et al. [49] to model THG from an array of apertures in his experiment. Figure (3.4) and (3.5) shows the schematic and experimental set up used by Nezami in his THG nonlinear theory for a rectangular aperture array. Nezami experiment considered a current source $J_{3\omega} \propto E_{\omega}^{3}$ derived from transforming equation (3.14) into the frequency domain for the third harmonic polarization and comparing it to equation (3.9). This current source is used to generate the out-coupled third harmonic wave ($J_{3\omega} \cdot E_{3\omega}$) by applying Lorentz reciprocity theorem to integrate the overlapping fields over a given material volume. The total out-coupled THG from the aperture array in Nezami experiment was estimated to be:

$$\mathbf{THG} \propto \int_{gold} \boldsymbol{\chi}_{gold}^{(3)} \boldsymbol{E}_{3\omega} \cdot \boldsymbol{E}_{\omega}^{3} \, dV \tag{3.15}$$

Where $\chi_{gold}^{(3)}$ is the nonlinear susceptibility of the gold metamaterial, E_{ω} is the electric field of the fundament light and $E_{3\omega}$ is the electric field of the third harmonic.

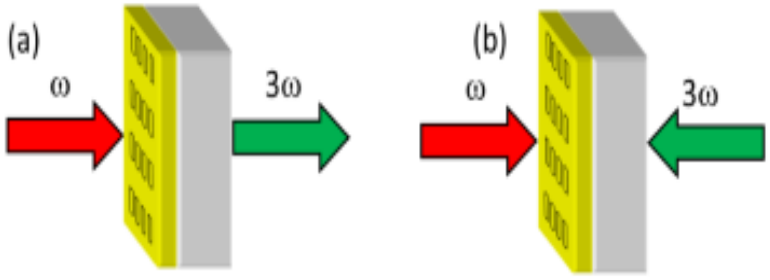

Figure 3.4: (a) Schematic of THG from a rectangular aperture array. (b) Illustration a simulated incident fundamental and third harmonic wave using time reversal for the harmonic beam. Reprinted with permission from Ref. [49]

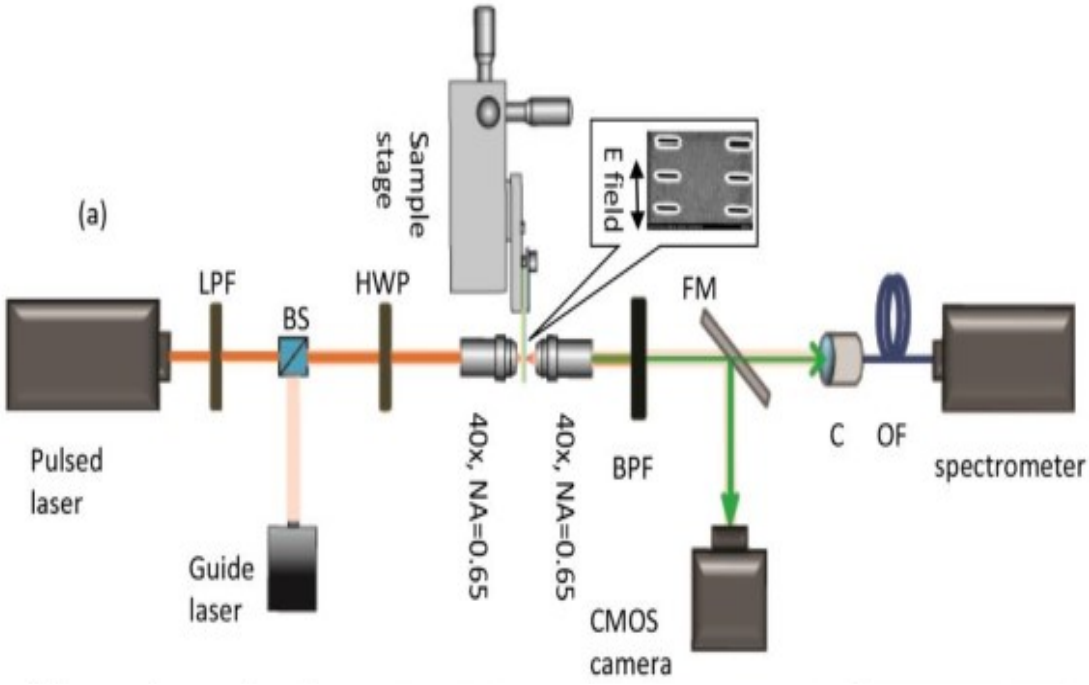

Figure 3.5: The schematic of the experimental set up used in reference [49] to investigate the localized and propagating surface plasmon in an aperture-based THG. Reprinted with permission from Ref. [49]

3.6 Plasmonics in Nonlinear Optics

The excitation of free electrons in a metal causing them to interact with the electromagnetic field is called plasmonics [56]. Marrtti et al. [57], explained the increasing effect of nonlinear optical response by plasmonics. He spoke about the various ways of enhancing the nonlinear optical effects by the application of plasmonics. Plasmonic effects on a metamaterial can result to either surface plasmon polaritons (SPPs) or localized surface plasmons (LSPs). LSP are common in the nano-metal particle whose resonance depends solely on the size and shape of the particle.

There are various advantages of the effect of plasmonics on nonlinear optics, some of which are the processing of optical signals at ultrafast speed and enhancement of optical

processes by producing a strong electromagnetic field. Gold is one of the widely used plasmonic materials because of its optical advantage. Of recent various research groups are looking into creating nonlinear plasmonic metamaterials with tunable optical properties [58].

3.7 Nonlinear Response of Metals

The effect of plasmonics on metals such as gold, to give a nonlinear interaction is a major theory in nonlinear optics. The nonlinear response of gold has become increasingly important, and this has driven various experiment to determine the accurate value for the third-order nonlinear optical susceptibility $\boldsymbol{\chi^{(3)}}$ of gold under various laboratory conditions. Bloembergen et al. [59], is said to be the first group that reported the nonlinear optical response of gold through the detection of third harmonic generation (THG). Recently, Boyd et al. [40] reported values obtained through experimental studies for the third-order nonlinear optical response of gold. Many groups reported various values for the third-order nonlinear optical response of gold, of which some of the values reported are incorrect [40]. The measurement of $\boldsymbol{\chi^{(3)}}$ depends mainly on the laboratory condition for which the value was obtained. The gold sample preparation procedure and the laser properties such as wavelength and pulse duration are the major constrains that would affect the value of $\boldsymbol{\chi^{(3)}}$ measured.

Table 3.1: Tabulated value for the third-order nonlinear optical response reported. Reprinted with permission from Ref. [40].

$\chi^{(3)}$ (m^2/V^2)	Method	τ_{pulse} (ps)	λ (nm)	n_2 (m^2/W)
7.71×10^{-19}	THG	30	1064	
2.45×10^{-19}	THG	30	1064	
$(-1.4+7i) \times 10^{-16}$	z-scan	30	532	$(14.8+7.0i) \times 10^{-14}$
$(-9.5+2.3i) \times 10^{-15}$	z-scan	30	532	$2.2i \times 10^{-12}$
$(3.7+5.0i) \times 10^{-14}$	z-scan	710	532	$(13.2-5.5i) \times 10^{-13}$
$(-15.4+1.3i) \times 10^{-18}$	z-scan	0.2	600	$5.73i \times 10^{-15}$
$(-76.8+4.3i) \times 10^{-20}$	z-scan	0.1	630	$3.41i \times 10^{-16}$
$(-75.7+4.2i) \times 10^{-18}$	z-scan	5.8	630	$3.36i \times 10^{-14}$
$(-0.39+2.2i) \times 10^{-16}$	z-scan	35	532	$(4.69+2.08i) \times 10^{-14}$
2.0×10^{-19}	FWM	0.2	800	

Fig. (3.6) shows the plot of the converted value of $\chi^{(3)}$ against the laser pulse duration using z-scan method by various groups. From fig. (3.6), a pulse duration of about 100 fs would result in a measurement of about 10^{-19} $m^{2/}V^2$ for $\chi^{(3)}$.

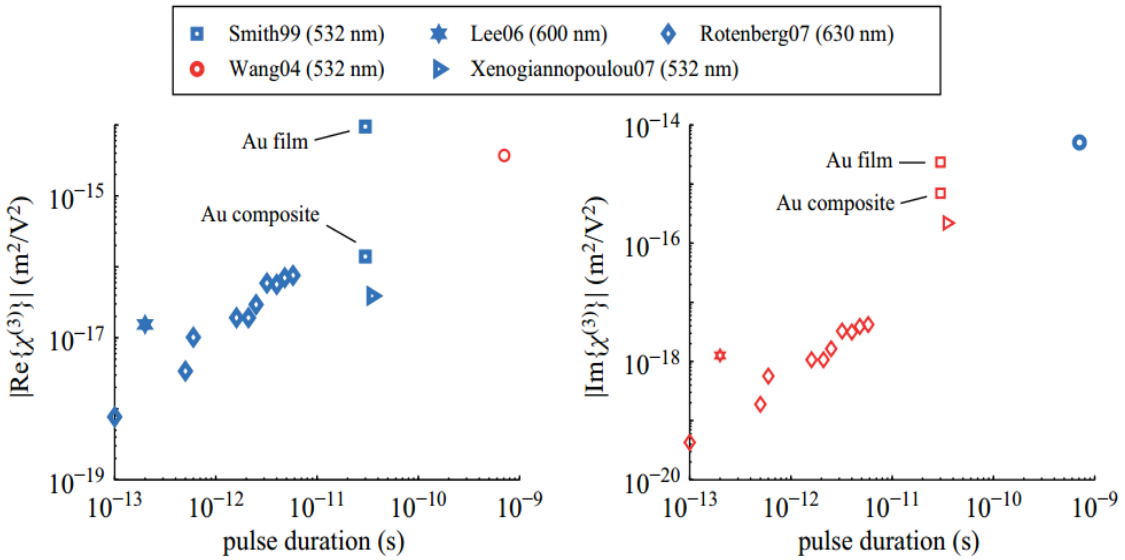

Figure 3.6: Plot of converted values of the third-order nonlinear susceptibility $\chi^{(3)}$ against the pulse duration of the laser using z-scan method. Reprinted with permission from Ref. [40]

Chapter 4: Simulation Design and Implementation

4.1 Introduction to Lumerical FDTD Simulation

Lumerical finite difference time domain (FDTD) can be defined as a high performance 3D FDTD-method that is used to solve Maxwell's equations for the design, analysis and optimization of nano-photonic devices and materials [60]. Some major applications of Lumerical FDTD are surface plasmons, metamaterials, solar cells and integrated optics.

Finite difference time domain (FDTD) is a vectorial method used to solve Maxwell's equations in complex geometries [60]. To implement an FDTD simulation, one would need to define a computational space and the material to use. The Lumerical FDTD simulation relies on the electromagnetic field and structural material in a time step that are related to the mesh size through the speed of light, to give a frequency domain and time domain results to the user. Hence, the application gives final information about the electric and magnetic field at a point or series of points within the specified computational space.

Like every other modeling applications Lumerical FDTD has its merits and demerits. The two major advantages of Lumerical FDTD in this project are:

I. Lumerical FDTD is user friendly, easy to understand and users know what to expect from their design.
II. Lumerical allows user to design their material structure and import their design into the computational space.

A major disadvantage in lumerical FDTD is the increase in simulation time and memory when considering accuracy in your simulation.

4.2 Model

The goal of this project is to investigate the detection of third harmonic generation, with respect to conversion efficiency in nano-apertures of a gold (Au) thin metal film and show that the FDTD nonlinear simulation agrees with both the experimental and linear simulation for nonlinear scattering theory. All simulations were performed using Lumerical FDTD solutions 8.12.501.

The effect of LSP and SPP resonances were applied to the structure to optimize the nonlinear conversion [49]. Based on the background study, the rate of conversion efficiency in a nonlinear material depends on the third order nonlinear susceptibility and the source power (intensity). Considering Nezami's [49] experimental set up, a gold film with a rectangular aperture is designed in Lumerical FDTD. In addition to the rectangular aperture design, other aperture shapes like double nano-hole (DNH) and H-shape were simulated to report the best shape that can produce the highest conversion efficiency.

4.2.1 Design Setup

In this simulation, we applied a previous design setup done by Nezami [49]. The design is composed of three layers of materials with different refractive index stacked up together. Fig. (4.1) shows the schematic of the design setup with gold, titanium and glass materials respectively and fig. (4.2) shows the schematic design of the three-aperture array used in this simulation. The design involves a plane wave source with wavelength of 1570 nm, and a focused on a spot size of 10 μm on a 100 nm thick gold film. A 5 nm thick Titanium (Ti) layer is used to glue the metamaterial to the glass to keep our metamaterial fixed on the glass.

Using periodic boundary condition and perfectly matched layer (PML), an aperture is carved into the gold surface and a monitor is placed in between the glass to collect the

transmitted fields. Fig. (4.3) and (4.4) shows the proposed design structure in Lumerical computational space surrounded by FDTD boundary with a mesh size of 1 nm.

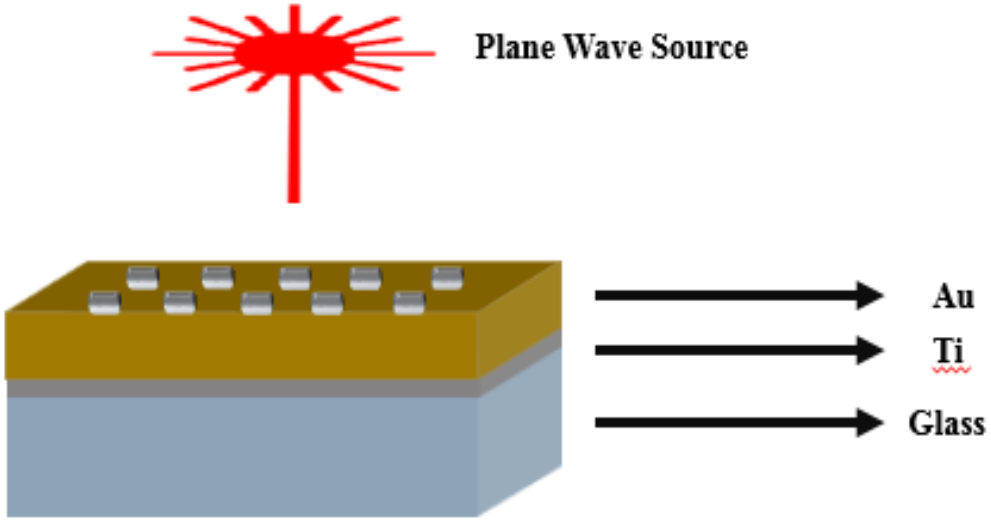

Figure 4.1: Schematic of the proposed design.

The refractive index of the gold material is tuned to third order nonlinear susceptibility with reference to Johnson and Christy experimental value for gold. Before running the simulation, the source, monitor, mesh and boundary conditions need to be set to the proper setting as specified in the appendix.

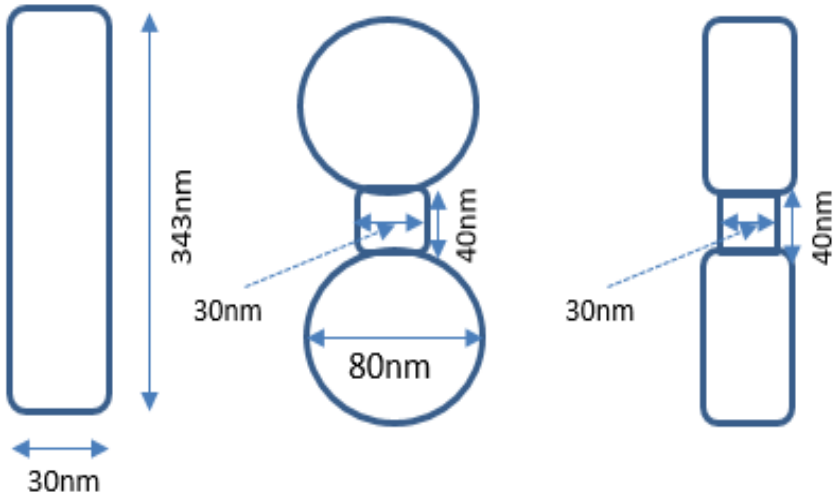

Figure 4.2: Rectangle, DNH and H-shape aperture array schematic

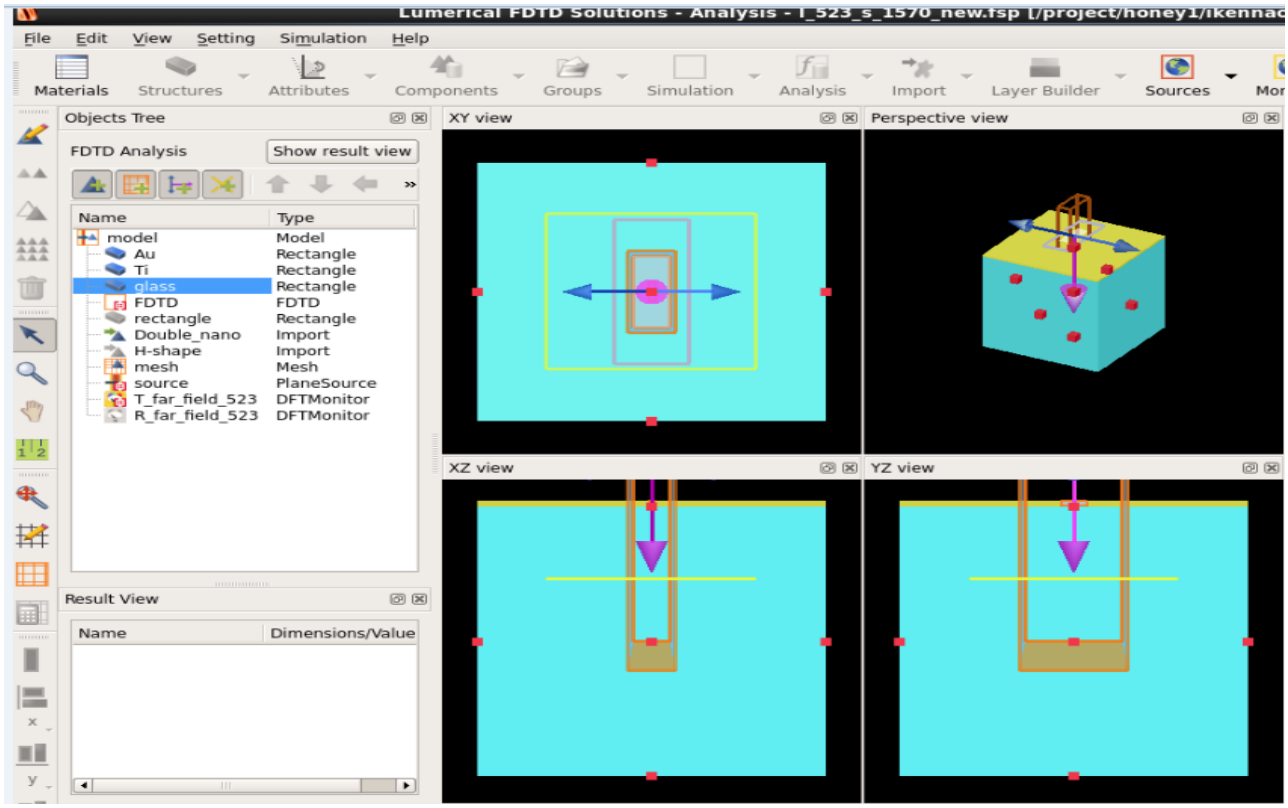

Figure 4.3: Platform of the Lumerical computation space

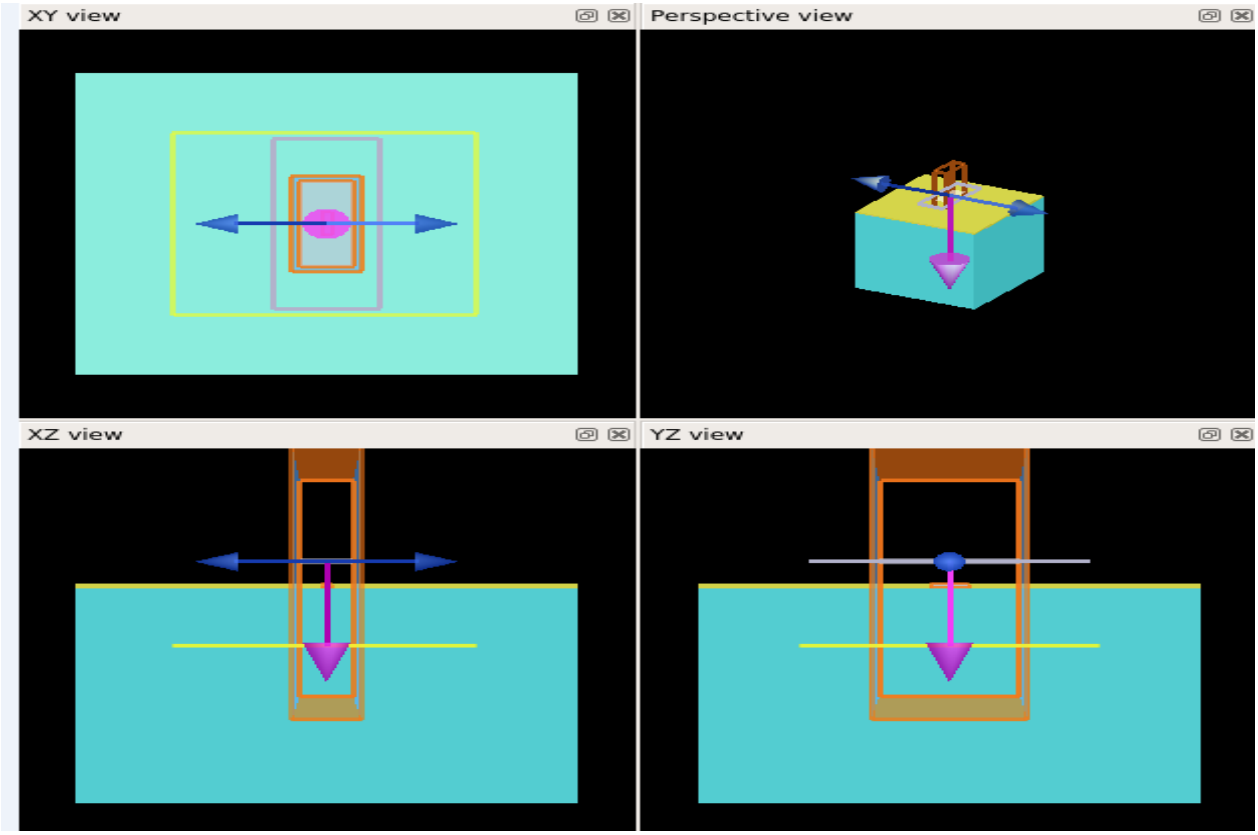

Figure 4.4: Proposed design in lumerical computational space

4.2.2 Nonlinear Methodology

Running nonlinear simulations is complicated in Lumerical as compared to running linear simulations. Therefore, lumerical has given some set of rules and conditions that one has to consider before running a nonlinear simulation. In this simulation, four major constrains that effect nonlinear simulation is discussed.

4.2.2.1 Source Amplitude.

For nonlinear simulations, the source amplitude is required to adjust the source to the desired value that would cause the nonlinear effect. This value can be calculated from the average incident power as shown in section (4.3). Lumerical advised that large source

amplitude could result in numerical instability hence rendering the polarization equation (3.2) invalid [60]. To correct this, the nonlinear terms must be smaller than the linear term as shown in equation (4.1).

$$\chi^{(3)}E^2 \ll \chi^{(1)} \tag{4.1}$$

4.2.2.2 Material Property

When running a nonlinear simulation, a new material is created and its properties need to be set to the corresponding third order nonlinear susceptibility. Fig. (4.5) shows the new material added to the material database for this simulation.

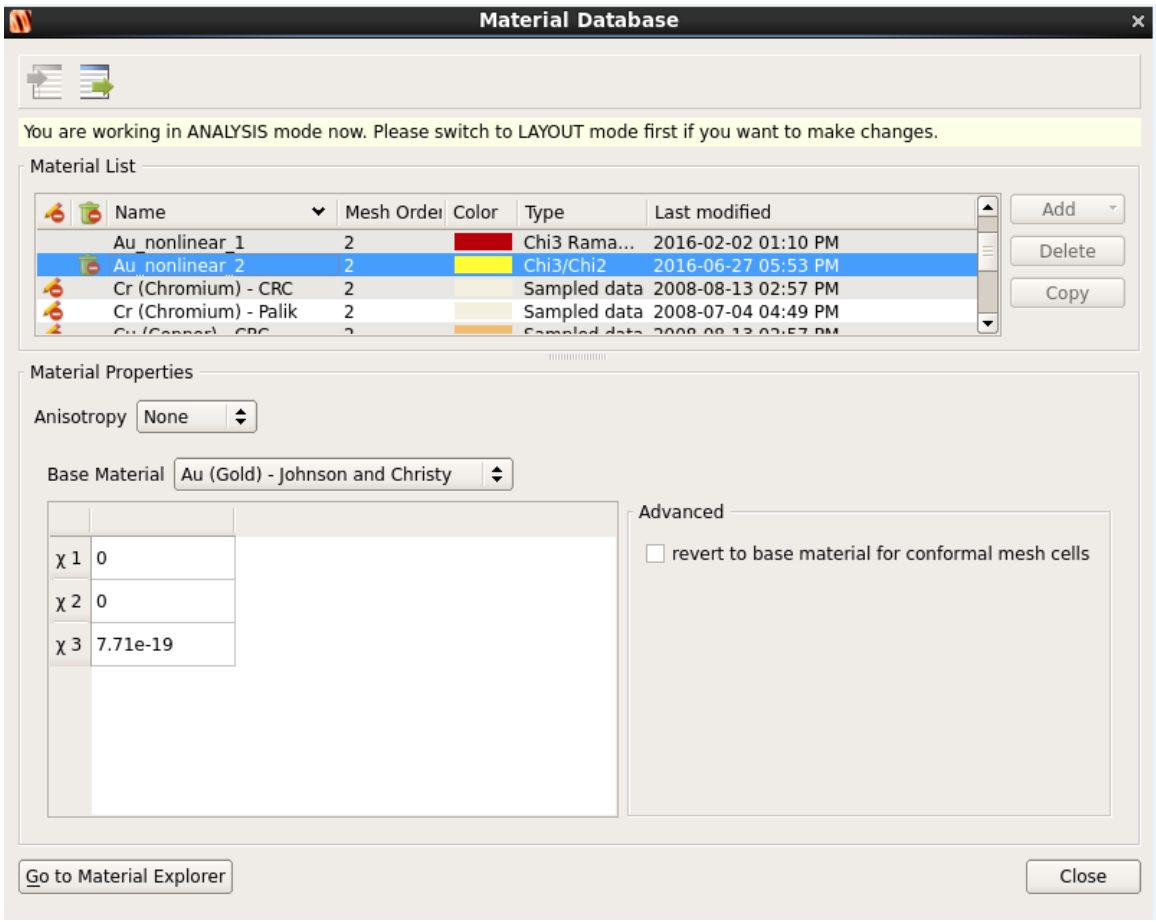

Figure 4.5: Properties settings of a gold material used

4.2.2.3 Power transmission

Reading the power transmitted from the monitor is different in nonlinear simulations. To read the average power from the frequency-domain field power monitor, we would have to use the transmission script (Poynting vector) that is defined in the Appendix (II).

4.2.2.4 Normalization

In Lumerical, the default setting is set to continuous wave (cw) normalization. One should note that the cw normalization is set to normalize the frequency monitor data to provide the cw steady state response of the system. This will not work for our nonlinear system, since the cw normalization mode reads the system to be in a linear mode. Hence, the use of no normalization (nonorm) was used in this project.

4.3 Theoretical calculations

Guided by the laser source power we have in the lab, the theoretical calculations for the simulation was carried out to obtain the amplitude. Considering a pulse rate of 100 fs with an average power of 40 mW, a repetition rate of 40 MHz and a spot size of 10 μm. We calculate the average intensity by using equation (4.2).

$$Avergae\ Intensity = \frac{P_{avg}}{Area} = 5.1 * 10^{8}\ Wm^{-2} \tag{4.2}$$

The peak intensity is defined as the ratio of the period between each pulse and the pulse rate multiplied by the average intensity.

$$Peak\ Intensity = \frac{Period}{Pulse\ rate} * Avg.Intensisty = 1.27 *\ 10^{14}\ Wm^{-2} \tag{4.3}$$

$$I = 0.5 * \varepsilon_o c E^2 \tag{4.4}$$

From equation (4.4) [62] we calculate the incident electric field in free space to be:

$$Amplitude = E_{1570} = \left(\frac{2I_{peak}}{\varepsilon_o c}\right)^{1/2} = 3.1 * 10^8\, Vm^{-1} \tag{4.5}$$

$$\vec{S} = \vec{E} \times \vec{H} \tag{4.6}$$

$$E \cdot \left(\nabla \times H = \vec{J} + \varepsilon_o \frac{d\vec{E}}{dt}\right) = -\nabla \cdot (E \times H) + H \cdot \left(\nabla \times E = -\mu_o \frac{d\vec{H}}{dt}\right) \tag{4.7}$$

$$Power = \int_v \vec{J} \cdot \vec{E}\ dv \tag{4.8}$$

Equation (4.6) is derived from Maxwell's equation (3.3-3.6), where electric field displacement and magnetic flux density is given to be $D = \varepsilon_o \vec{E}$ and $B = -\mu_o \vec{H}$ respectively. From the derivation of Poynting theorem using Maxwell's equation (4.7), we calculated the rate at which the current density with a corresponding electric field works on the proposed structure over a given volume as shown in equation (4.8). The output power was calculated using poynting vector [61-62] from the transmission monitor and integrated over area X and Y to obtain the average output power. Since the simulation is carried out in a nonorm mode, the output power normalization unit is in Watts/Hz^2. Equation (4.9) was used to normalize the output power to (Watts), hence enabling one to calculate the conversion efficiency using equation (4.10).

$$F^2 = \left(c/\lambda\right)^2 = \left(\frac{3 \times 10^8\, ms^{-1}}{0.523 \times 10^{-6}\, m}\right)^2 = Hz^2 \tag{4.9}$$

$$Conversion\ efficiency = \frac{Output\ power}{Input\ power} \times 100\% \tag{4.10}$$

4.4 Results and Discussion

In this report, we compare the FDTD nonlinear simulation result to the experimental and linear THG simulation carried out by Nezami. Based on recent research works that looked into the effect of LSP resonance on SHG [63-65] and THG [49]. Three aperture shapes were simulated and the aperture shape with the highest conversion efficiency was reported. From the nonlinear simulation results, one can see that the conversion efficiency depends on the intensity (avg. excitation power) and the third order nonlinear susceptibility value of the gold material with respect to the periodicity of the aperture array. The table below shows the values used in this simulation.

Table 4.1: Parameter Value

Parameter	Value
Pulse Rate	100 Fs
Repetition Rate	40 MHz
Spot Size	10 μm
Permittivity of vacuum ε_o	8.85×10^{-12} F/m
Speed of light	$3 \times 10^{8}\ ms^{-1}$
Refractive index of Glass	1.52
Third order nonlinear susceptibility	$7.71 \times 10^{-19}\ m^2/V^2$
Average power	40 mW

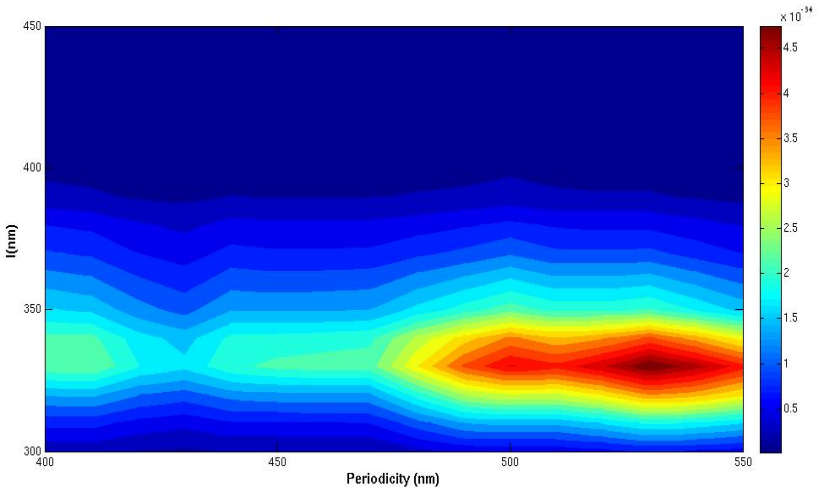

Figure 4.6: LSP resonance at 1570 nm and propagation SPP at 523 nm

Figure (4.6) shows the THG in natural logarithm scale when we tune the LSP resonance to 1570 nm and the SPP resonance to 523 nm using the nonlinear scattering theory in Equation (3.14). In fig. (4.7), a rectangular aperture array of diameter 30 nm with an input power ranging from 40 mW to 0.417 W was used to plot the logarithmic ratio of the input average power to output average power. From the simulation result, it was discovered that using an amplitude that ranges from 10^8 to 10^9 Vm^{-1} is enough to cause a nonlinear effect on the 100 nm thick gold metamaterial. A good advantage of this nonlinear simulation over past simulation works in nonlinear scattering theory, is the fact that the simulation can produce results when simulating for higher powers to investigate the saturation point as shown in the fig. (4.8).

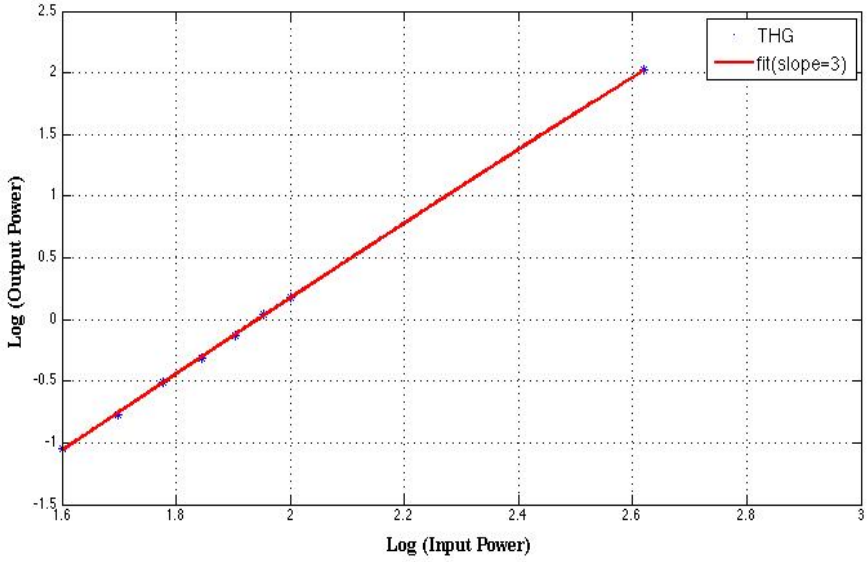

Figure 4.7: Ratio of input average power to output power in logarithm scale (dB)

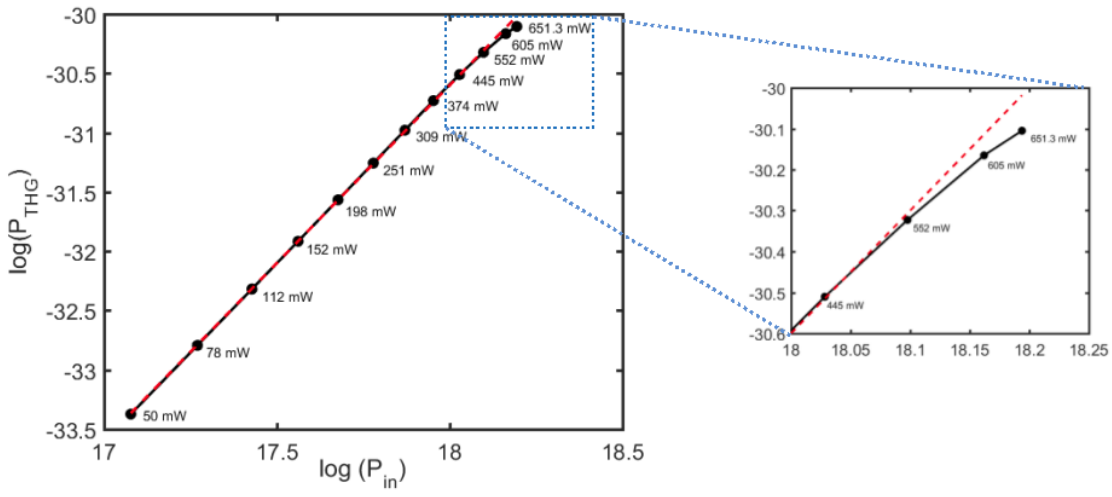

Figure 4.8: Output THG power as a function of incident power for an array of rectangular aperture normalized in logarithm scale (dB).

Figure (4.8) shows the effect of higher incident power (black curve) on a rectangular aperture array with a periodicity of 528 nm. The corresponding average incident power is shown by the data points. Increasing the amplitude to as high as 1.2×10^{9} Vm^{-1} using a third order nonlinear susceptibility of $7.71\times10^{-19}\ m^2/V^2$, we approach a damage threshold where the value for the output power becomes invalid. The reason behind this can be found in section 4.2.2.1, where the source amplitude is bounded by its proportionality to the linear susceptibility of the material. Figure (4.9) shows that a diameter of about 30x343 nm would produce a high conversion efficiency in a rectangular aperture of the proposed design. This is because, using a periodicity of 528 nm, a resonance would be observed using a diameter of 30 nm as we approach a length of about 343 nm. These results were obtained under an average input power of 40 mW and a third order nonlinear susceptibility of $7.71\times10^{-19}\ m^2/V^2$. This result gives an insight on how to module other aperture array sizes.

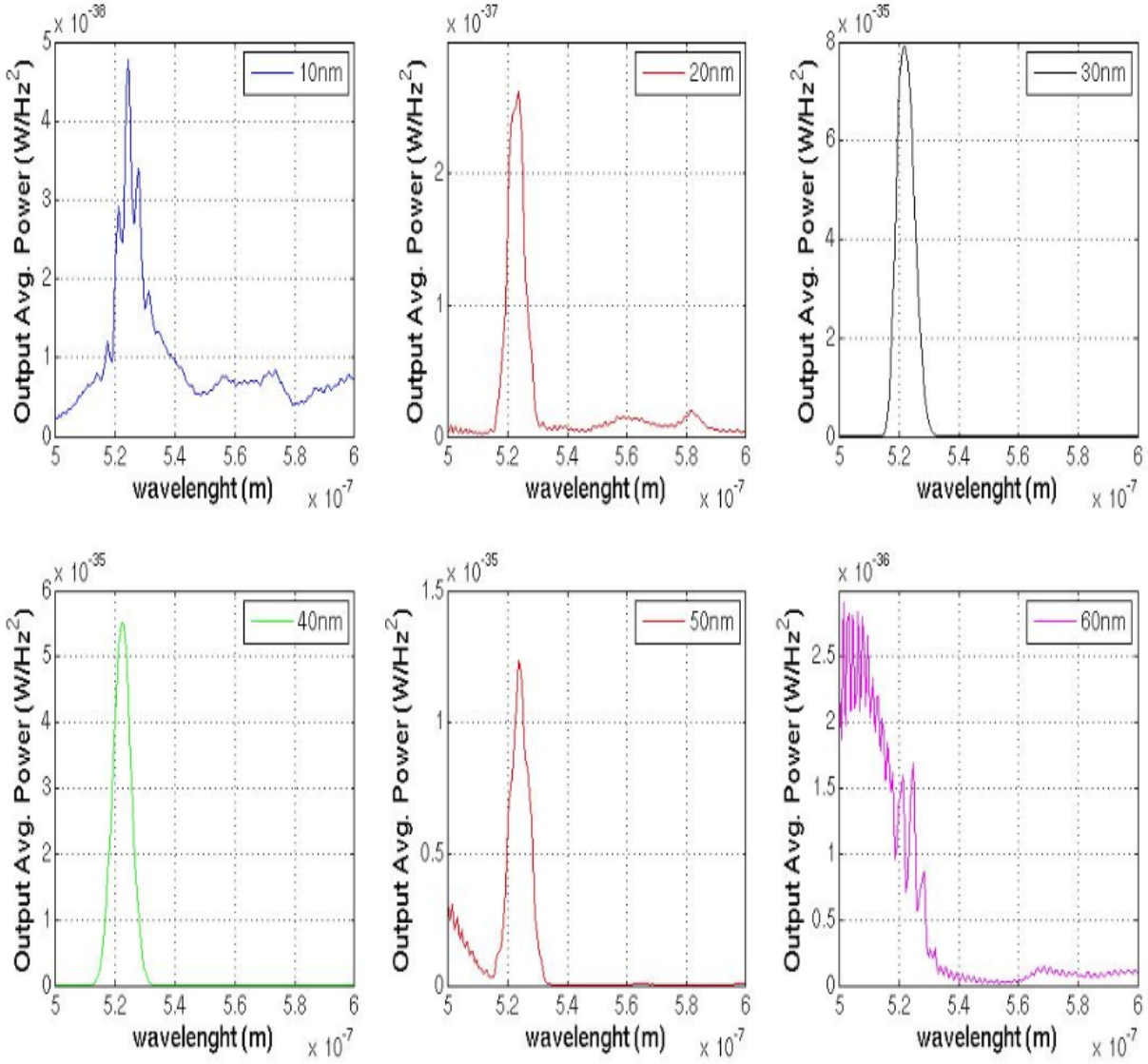

Figure 4.9:THG with a periodicity of 528 nm from a rectangular aperture

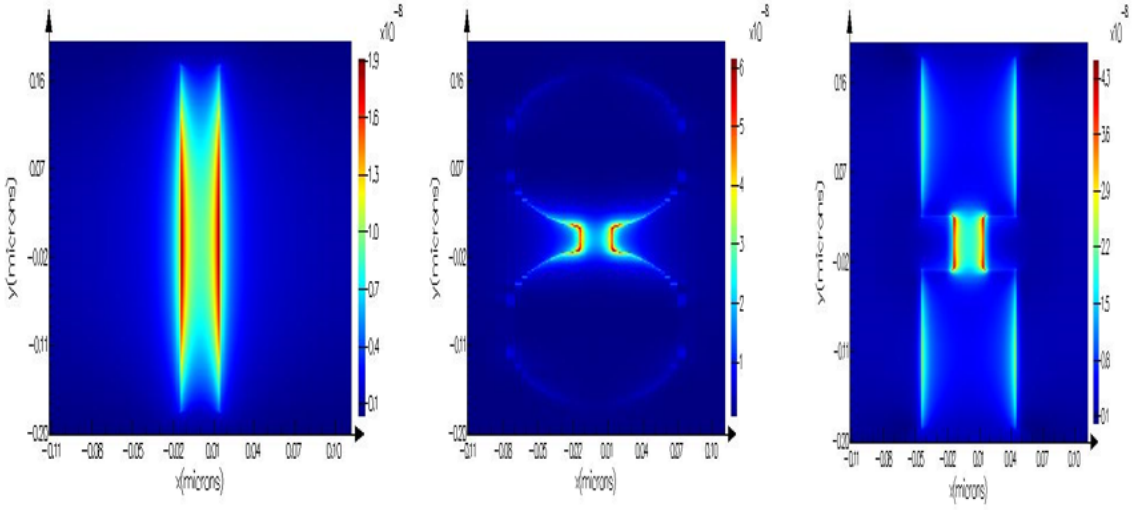

Figure 4.10: Electric field magnitude and distribution for a 30 nm gap at third harmonic wavelength of 523 nm for rectangular, DNH and H-shape aperture array respectively.

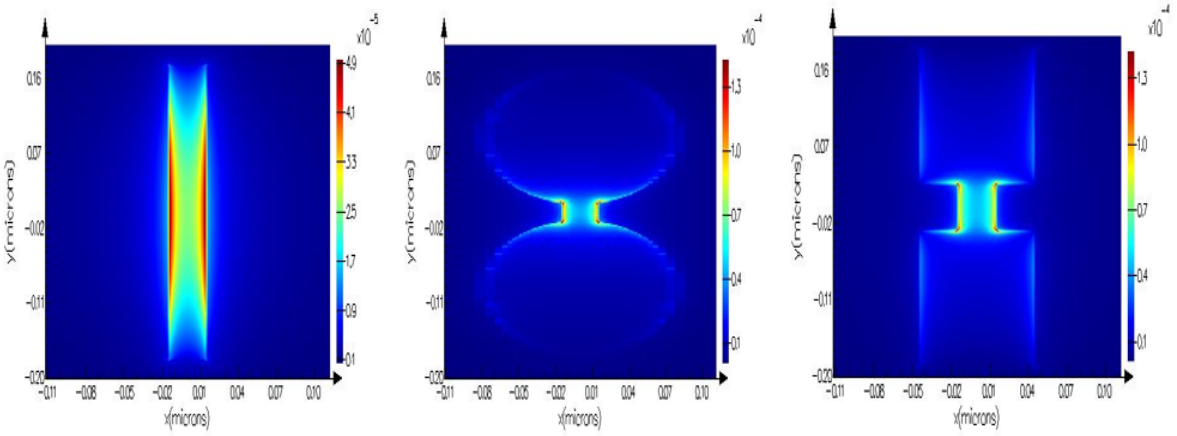

Figure 4.11: Electric field magnitude and distribution for a 30 nm gap at fundamental wavelength of 1570 nm for rectangular, DNH and H-shape aperture array respectively.

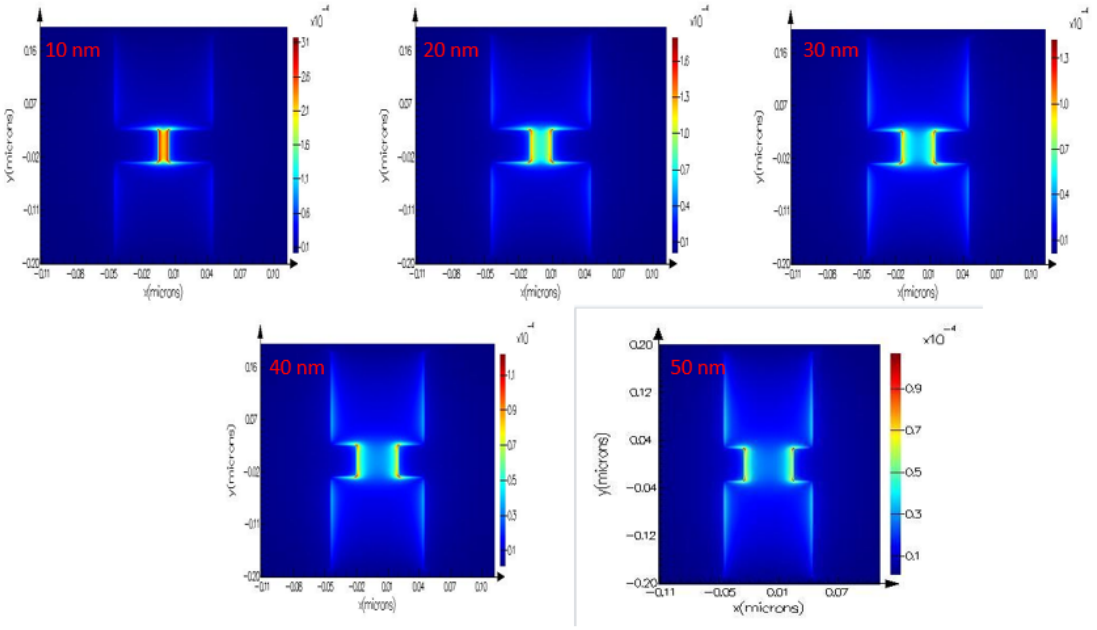

Figure 4.12: Electric field distribution in H-shape aperture array at third harmonic wavelength of 523 nm.

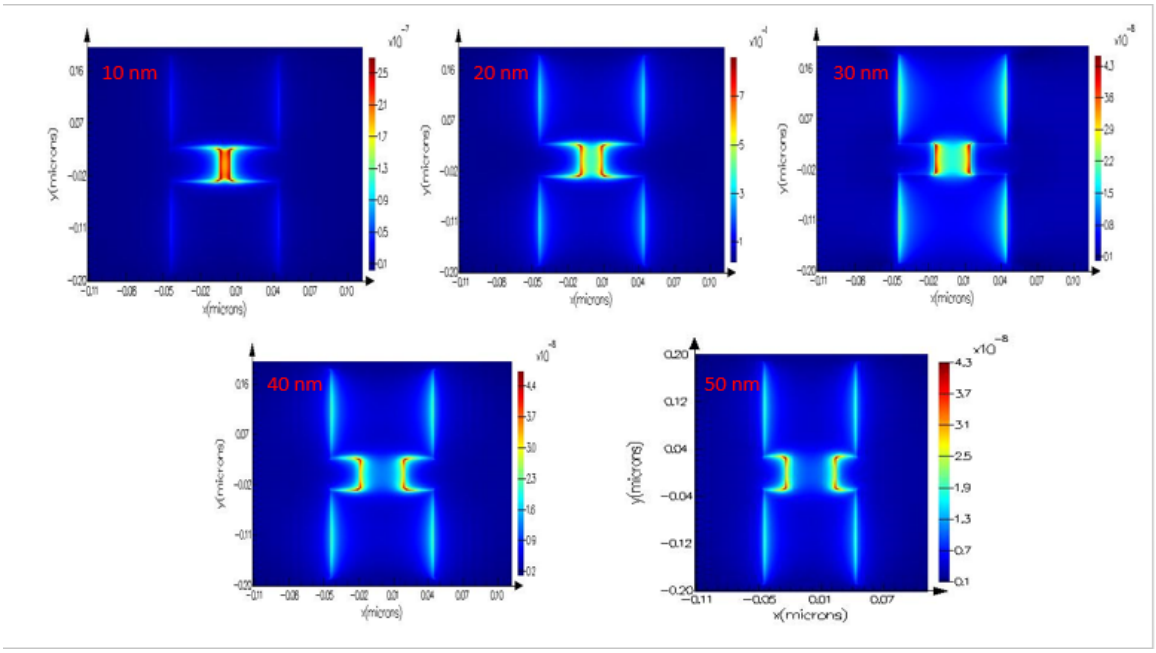

Figure 4.13: Electric field distribution in H-shape aperture array at fundamental wavelength of 1570 nm.

With recent research works showing that the aperture shape can vary the LSP resonance to yield a higher conversion efficiency for a metal film [18, 22], the rectangular shape was compared to DNH and H-shape to show which aperture shape would produce the highest conversion efficiency. The electric field distribution and magnitude for three aperture array at third harmonic and fundamental wavelengths is shown in fig. (4.9) and (4.10). This result shows that the H-shape aperture is the optimal structure and fig. (4.11) and (4.12) shows the variation in geometry at third harmonic and fundamental wavelength of the optimal structure with respect to the electric field magnitude and distribution.

Figure (4.13) and (4.14) shows the detection of THG in 100 nm thick gold metasurface material using a DNH array of periodicity 420 nm, rectangular array and H-shaped array of periodicity 528 nm. A mesh size of 1 nm was used to produce this result to ensure that the convergence limit is reached. From the results shown below it is easy to see that H-shape aperture array would produce the highest conversion efficiency of about 0.52 % as shown in table 4.2.

Table 4.2: Result showing the conversion efficiency for the three aperture shapes.

Aperture Shape	Amplitude |E|	Intensity(Wm^{-2})	Conversion Efficiency (%)
H-shape	3.1×10^{8}	1.273×10^{14}	0.52
DNH	3.1×10^{8}	1.273×10^{14}	0.12
Rectangular	3.1×10^{8}	1.273×10^{14}	0.061

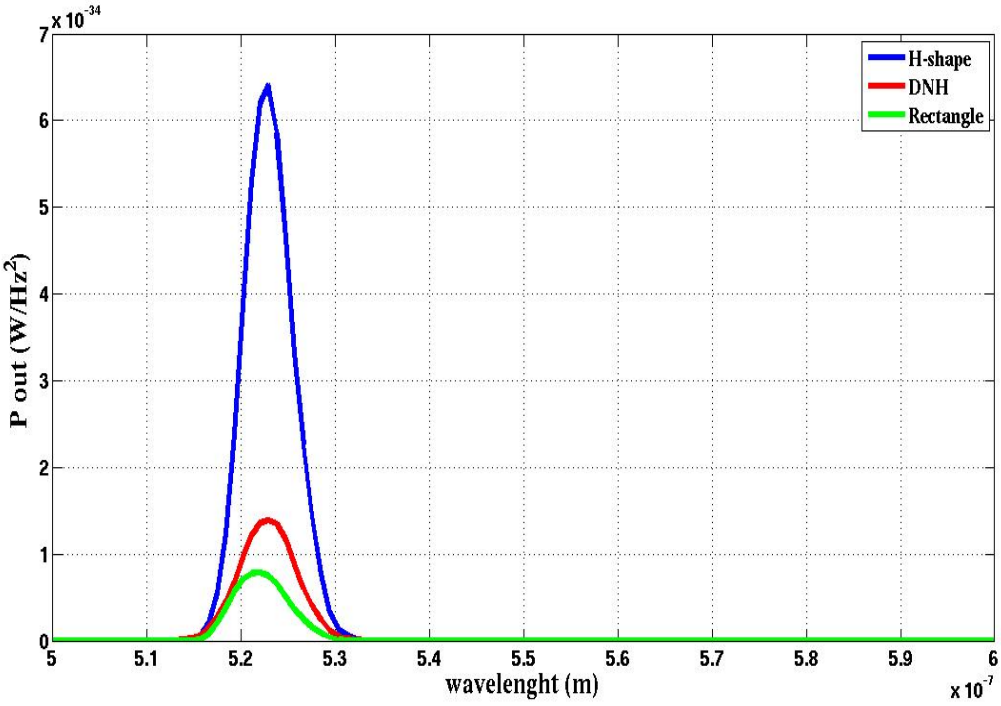

Figure 4.14: THG with respect to average output power

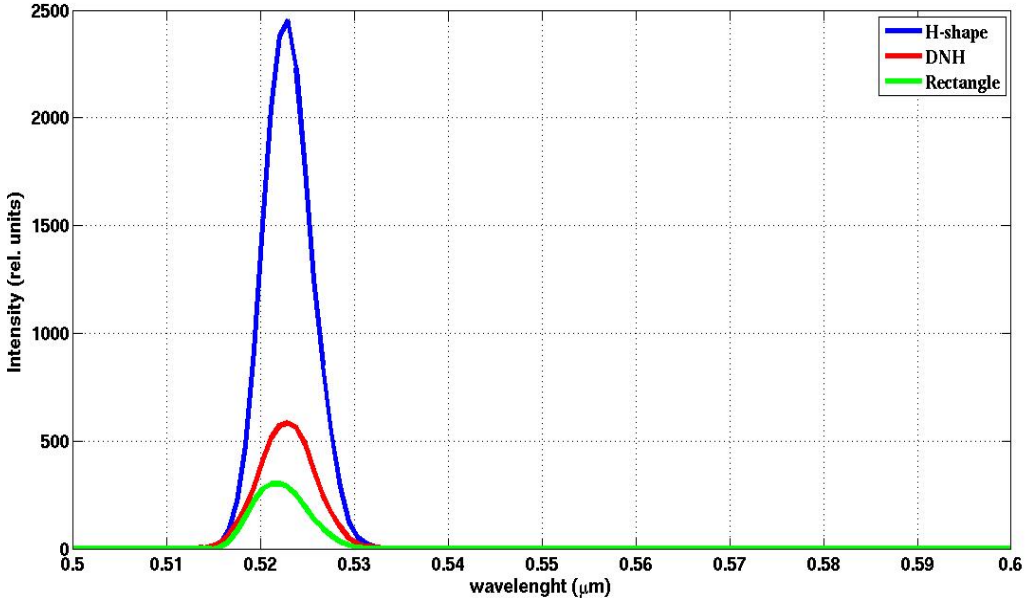

Figure 4.15: Transmission ratio of THG in three different apertures

Table 4.3 shows the quantitative comparison of the nonlinear scattering theory used by Nezami [66] in his experiment and the FDTD nonlinear simulation theory. The FDTD nonlinear theory shows a good agreement with both the experimental result and the linear simulation result. Comparing the linear simulation to the nonlinear simulations, the nonlinear simulation method is better than the linear simulation when considering simulating for higher powers and studying the effect of a change in the third order nonlinear susceptibility value $\chi^{(3)}$ of the metasurface material. Also, since the linear simulation is computationally intensive, the linear simulation requires more memory than the nonlinear simulation that produces the result instantly

Table 4.3: Comparison of reported experimental and linear simulation results to nonlinear simulation result.

Structure	Normalized nonlinear experiment [66]	Normalized linear simulation [66]	Normalized non-linear simulation (40 mW)
H-shaped array	1	1	1
DNH array	0.20	0.24	0.23
Rectangular array	0.10	0.13	0.12

Chapter 5: Conclusion and Future works

5.1 Conclusion

In this project, a nonlinear FDTD simulation method used to detect third harmonic generation was proposed. The proposed nonlinear simulation method utilizes the effect of localised surface plasmon (LSP) reasonance and surface plasmon polariton (SPP) to increase the detection of THG. The simulation method also agrees with the report by Nezami et al. [66] and shows that the H-shape aperture would give a maximum conversion efficiency of 0.52 %, which is about ten times higher than what was reported when a rectangular aperture was used [49].

Finally, the simulation results show that the FDTD nonlinear scattering simulation agrees with the nonlinear scattering theory from the experiment. This further goes to show that one can successfully carry out a nonlinear simulation with Lumerical FDTD under well-defined settings.

5.2 Future works

The detection of third harmonic generation (THG) depends on the intensity of the laser and the third order nonlinear susceptibility of the metal material. Further investigation in terms of experiment needs to be carried out to discover the true value of the third order nonlinear susceptibility of the gold metamaterial using wavelength of 1570 nm. The stability factor of nonlinear simulation has to be investigated to determine how far one could reach before the simulations diverges.

In addition, Melentiev et al. [22] has shown that aluminum (Al) can give a high conversion efficiency that is three orders of magnitude higher than gold on a single

nanoslit. One can try to simulate the proposed design in this project using Aluminum (Al) as the metamaterial instead of gold.

Bibliography

1. Robert W. Boyd, “Nonlinear Optics,” Third Edition, Academic press, ISBN 978-0-12-369470-6 (2008).
2. M. Kauranen and A. V. Zayats, “Nonlinear plasmonics,” Nat. Photonics 6(11), 737–748 (2012).
3. M. Ren, B. Jia, J.-Y. Ou, E. Plum, J. Zhang, K. F. MacDonald, A. E. Nikolaenko, J. Xu, M. Gu, and N. I. Zheludev, “Nanostructured plasmonic medium for terahertz bandwidth all-Optical switching,” Adv. Mater. 23(46), 5540–5544 (2011).
4. C. Min., Pei Wang, C. Chen, Y. Dang, Y. Lu, H. Ming, T. Ning,Y. Zhou, and G. Yang, “All-optical switching in subwavelength metallic grating structure containing nonlinear optical materials,” Opt. Lett. 33(8), 869-871 (2008).
5. A. Nahata, R. A. Linke, T. Ishi, and K. Ohashi, “Enhanced nonlinear optical conversion from periodically nanostructured metal film,” Opt. Lett. 28(6), 423-425 (2003).
6. S.Palomba and L.Novotny, “Near-field imaging with localized nonlinear source,” Nano Lett.9 (11), 3801-3804 (2009).
7. P.-Y. Chen and A. Alù, “Subwavelength imaging using phase-conjugating nonlinear nanoantenna arrays,” Nano Lett. 11(12), 5514–5518 (2011).
8. P. A. Franken, A. E. Hill, C. W. Peters, and G. Weinreich, “Generation of optical harmonics”, Phys. Rev. Lett. 7, 118-119 (1961).
9. Robert L. Byer, “Nonlinear optical phenomena and materials”, Annual review of Materials Science vol. 4, 147-190 (1974).
10. E. Almeida. G. Shalem, and Y. Prior, “Subwavelength nonlinear phase control and anomalous phase matching in plasmonic metasurfaces”, Nat. Commun. 7:10367 doi: 10.1038/ncomms10367 (2016).
11. N. Yu and F. Capasso, “Flat optics with designer metasurfaces”, Nat. Mater.13, 139-150 (2014).
12. V. Kildishev, A. Boltasseva, and V. M. Shalaev, “Planar photonics with metasurfaces”, Science 339, 1232009 (2013).
13. Lesuffleur, L. K. S. Kumar, and R. Gordon, “Apex-enhanced second-harmonic generation by using doublehole arrays in a gold film,” Phys. Rev. B 75(4), 045423 (2007).
14. K. Canfield, H. Husu, J. Laukkanen, B. Bai, M. Kuittinen, J. Turunen, and M. Kauranen, “Local field asymmetry drives second-harmonic generation in non-centrosymmetric nanodimers,” Nano Lett. 7(5), 1251– 1255 (2007).
15. J. C. Prangsma, D. Oosten, R. J. Moerland, and L. Kuipers, “Increase of group delay and nonlinear effects with hole shape in subwavelength hole arrays,” New J. Phys. 12(1), 013005 (2010).
16. J. A. H. van Nieuwstadt, M. Sandtke, R. H. Harmsen, F. B. Segerink, J. C. Prangsma, S. Enoch, and L. Kuipers, “Strong modification of the nonlinear optical response of metallic subwavelength hole arrays,” Phys. Rev. Lett. 97(14), 146102 (2006).

17. L. Wang, R. Wang, R. J. Liu, X. H. Lu, J. Zhao, and Z.-Y. Li, "Origin of shape resonance in second-harmonic generation from metallic nanohole arrays," Sci. Rep. 3, 2358 (2013).
18. W. Fan, S. Zhang, K. J. Malloy, S. R. J. Brueck, N. C. Panoiu, and R. M. Osgood, "Second harmonic generation from patterned GaAs inside a subwavelength metallic hole array," Opt. Express 14(21), 9570–9575 (2006).
19. H. Barakat, M.-P. Bernal, and F. I. Baida, "Second harmonic generation enhancement by use of annular aperture arrays embedded into silver and filled by Lithium Niobate," Opt. Express 18(7), 6530–6536 (2010).
20. T. Thio, H. J. Lezec, T. W. Ebbesen, K. M. Pellerin, G. D. Lewen, A. Nahata, and R. A. Linke, "Giant optical transmission of sub-wavelength apertures: physics and applications," Nanotechnology 13(3), 429–432 (2002).
21. P. N. Melentiev, T. V. Konstantinova, A. E. Afanasiev, A. A. Kuzin, A. S. Baturin, A. V. Tausenev, A. V. Konyaschenko, and V. I. Balykin, "Single nano-hole as a new effective nonlinear element for third-harmonic generation," Laser Phys. Lett. 10(7), 075901 (2013).
22. P. N. Melentiev, A. E. Afanasiev, A. A. Kuzin, A. S. Baturin, and V. I. Balykin, "Giant optical nonlinearity of a single plasmonic nanostructure," Opt. Express 21(12), 13896–13905 (2013).
23. P. N. Butcher and D. Cotter, "The Elements of Nonlinear Optics", Cambridge Univ. Press, New York, 1990.
24. T.H. Maiman, "Stimulated optical radiation in ruby", Nat. (187), 493-494 (1960).
25. M. Bass, P. A. Franken, A. E. Hill, C. W. Peters, and G. Weinreich, "Optical Mixing", Phys. Rev., vol. 8, p. 18 (1962).
26. P. D. Maker, R. W. Terhune, M. Nisenhoff, and C. M. Savage, "Effects of dispersion and focusing on the production of optical harmonics," Phys. Rev. Lett. 8, 21-22 (1962).
27. N. Bloembergen and Y. R. Shen, "Quantum theoretical comparison of nonlinear susceptibilities parametric media, lasers, and raman lasers," Phys. Rev. 133, A37-A49 (1964).
28. J. A. Armstrong, N. Bloembergen, J. Ducuing, and P. S. Pershan, "Interactions between light waves in a nonlinear dielectric", Phys. Rev. 127, 1918-1939 (1962).
29. J. A. Giordmaine, "Mixing of light beams in crystal", Phys. Lett. 8, 19-20 (1962).
30. G. Eckardt, R. W. Hellwarth, F. J. McClung, S. E. Schwartz, D. Weiner, and E. J. Woodbury, "Stimulated Raman scattering from organic liquids", Phys. Rev. 9, 455 (1962).
31. K. Yee, "Numerical solution of initial boundary value problems involving Maxwell's equations in isotropic media", IEEE Trans. on Ante. and Prop. 14(3): 302-307 (1966).
32. Taflove, "Application of the finite-difference time-domain method to sinusoidal steady state electromagnetic penetration problems", IEEE Trans. on Electrom. Comp. EMC-22 (3), 191-202 (1980).
33. Renger, R. Quidant, N. van Hulst, and L. Novotny, "Surface-enhanced nonlinear four-wave mixing," Phys. Rev. Lett. 104(4), 046803 (2010).
34. S. Palomba, M. Danckwerts, and L. Novotny, "Nonlinear plasmonics with gold nanoparticle antennas", J. Opt. A: Pure Appl. Opt. 11, 114030 (2009).

35. Bouhelier, M. Beversluis, A. Hartschuh, and L. Novotny, "Near field Second harmonic induced by local field enhancement", Phys. Rev. Lett. Vol. 90, 13903 (2003).
36. G. S. Agarwal and S. S. Jha, "Theory of second harmonic generation at a metal surface with surface plasmon excitation," Solid State Commun. 41(6), 499–501 (1982).
37. H. J. Simon, D. E. Mitchell, and J. G. Watson, "Optical second-harmonic generation with surface plasmons in silver films," Phys. Rev. Lett. 33(26), 1531–1534 (1974).
38. S. Kim, J. Jin, Y. Kim, Y. Park, Y. Kim, and S. Kim, "High-harmonic generation by resonant plasmon field enhancement", Nat. Lett. 453, 757-760 (2008).
39. K. O'Brien, H. Suchowski, J. Rho, A. Salandrino, B. Kante, X. Yin, and X. Zhang, "Predicting nonlinear properties of metamaterials from the linear response," Nat. Mater. 14(4), 379–383 (2015).
40. R. W. Boyd, Z. Shi, and I. D. Leon, "The third-order nonlinear optical susceptibility of gold", Opt. Comm. 326, 74-79 (2014).
41. M. Airola, Y. Liu, and S. Blair, "Second-harmonic generation from an array of sub-wavelength metal apertures," J. Opt. A, Pure Appl. Opt. 7(2), 118 (2005).
42. K. D. Ko, A. Kumar, K. H. Fung, R. Ambekar, G. L. Liu, N. X. Fang, and K. C. Toussaint, Jr., "Nonlinear optical response from arrays of Au bowtie nanoantennas," Nano Lett. 11(1), 61–65 (2011).
43. S. G. Rodrigo, V. Laliena, and L. Martín-Moreno, "Second-harmonic generation from metallic arrays of rectangular holes," J. Opt. Soc. Am. B 32(1), 15–25 (2015).
44. T. Xu, X. Jiao, G. P. Zhang, and S. Blair, "Second-harmonic emission from sub-wavelength apertures: Effects of aperture symmetry and lattice arrangement," Opt. Express 15(21), 13894–13906 (2007).
45. O. Wolf et al, "Phased array sources based on nonlinear metamaterial nanocavities", Nat. Commun. 6, 7667 (2015).
46. T. Xu, X. Jiao, and S. Blair, "Third-harmonic generation from arrays of sub-wavelength metal apertures," Opt. Express 17(26), 23582–23588 (2009).
47. M. Lippitz, M. A. V. Dijk, and M. Orrit, "Third Harmonic generation from single gold nanoparticles", Nano Lett. 5, 799-802 (2005).
48. G. Hajisalem, D. K. Hore, and R. Gordon, "Interband transition enhanced third harmonic generation from nanoplasmonic gold," Opt. Mater. Express 5(10), 2217–2224 (2015).
49. M. S. Nezami, and R. Gordon, "Localized and propagating surface plasmon resonances in aperture-based third harmonic generation", Opt. Exp. 23, 32006-32014 (2015).
50. T. V. Konstantinova, P. N. Melent'ev, A. E. Afanas'ev, A. A. Kuzin, P. A. Starikov, A. S. Baturin, A. V. Tausenev, A. V. Konyashcenko, and V. I Balykin, "A Nanohole in a thin Metal Film as an Efficient nonlinear optical element", J. of Exp. and Theore. Phys. Vol. 117, 21-31 (2013).
51. S. Roke, M. Bonn, and A. V. Petukhov, "Nonlinear optical scattering: The concept of effective susceptibility", Phys. Rev. B 70(11), 115106(2004).

52. A. G. de Beer, and S. Roke, “Nonlinear Mie theory for second harmonic and sum frequency scaterring”, Phys. Rev. B 79(15), 155420 (2009).
53. Y. R. Shen, “The Principles of Nonlinear optics”, John Wiley and Sons, 2002.
54. S.V. Fomichev, and W. Becker, “Linear and nonlinear scattering and absorption in free-electron nanoclusters with diffuse surface:General considerations and linear response”, Phys. Rev. A 81, 063201 (2010).
55. C. F. Hernadez, G. R. Ortiz, S. Y. Tseng, M. P. Gaj, and B. Kippelen, “Third harmonic generation and its applications in optical image processing”, J. Mater. Chem. 19, 7394-7401 (2009).
56. S. A. Maier, “Plasmonics: Fundamentals and applications”, Springer, 978-0-387-37825-1 (2007).
57. M. Kauranen, and A. V. Zayats, “Nonlinear plasmonics”, Nat. Photonics 6, 737-748 (2012).
58. Y. H. Ye, Y. J. Huang, W. T. Lu, B. D. F. Casse, D. Xiao, S. P. Bennett, D. Heiman, L. Menon, and S. Sridhar, “Tuning the optical properties of metamaterials based on gold nanowire arrays embedded in alumnia”, Opt. Mat. 33, 1667-1670 (2011).
59. N. Bloembergen, W. K. Burns, and M. Matsuoka, “Reflected third harmonic generated by picosecond laser pulses”, Optics Comm. vol. 1(4), 195-198 (1969).
60. Lumerical. Lumerical Solutions, Inc. Availabe at http://www.lumerical.com/tcad-products/fdtd (2014).
61. J. Weiner, and F. Nunes, “Light-matter interaction: Physics and engineering at nanoscale”, Oxford University Press, 2013.
62. P. N. Butcher,and D. Cotter, “The Elements of Nonlinear Optics”, Cambridge University Press Revised edition, 1991.
63. A. Salomon, M. Zielinski, R. Kolkowski, J. Zyss and Y. Prior, “Size and shape resonances in second harmonic generation from silver nanocavities”, J. Phys. Chem. 117(43), 22377-22382 (2013).
64. P. Genevet, J. Tetienne, E. Gatzogiannis,R. Blanchard, M. Kats, M. Scully and F. Capasso, “Large enchancement of nonlinear optical phenomena by plasmonic nanocavity gratings”, Nano Lett. 10, 4880-4883 (2010).
65. B. Wang, R. Wang, R. Lui, X. Lu, J. Zhao and Z. Li, “Origin of shape resonance in second harmonic generation metallic nanohole arrays”, Sci. Rep. 3, 2358 (2013).
66. M. S. Nezam, D. Yoo, G. Hajisalem, S. H. Oh, and R. Gordon, “Gap plasmon enhanced metasurface third-harmonic generation in transmission geometry”, ACS Phot., (2016).

Appendix A: Settings and Configurations

I. Source

There are various sources in the Lumerical plat form. For the sake of this project, a plane wave source was used to inject electromagnetic energy from one side of the source region along the plane. Once a source is selected, the location, propagation direction, frequency/wavelength and amplitude of the source can be edited to the required setting. Fig. (A.1 – A.3) shows the configuration of the plane wave source at an average power of 40mw, propagating at a wavelength of 1570nm. From fig. (A.3), using pulse duration of 100fs, one would have set a pulse offset that is at least twice the pulse duration [60]. Section 4.3 discussion the calculation and pulse length for the power source in detail.

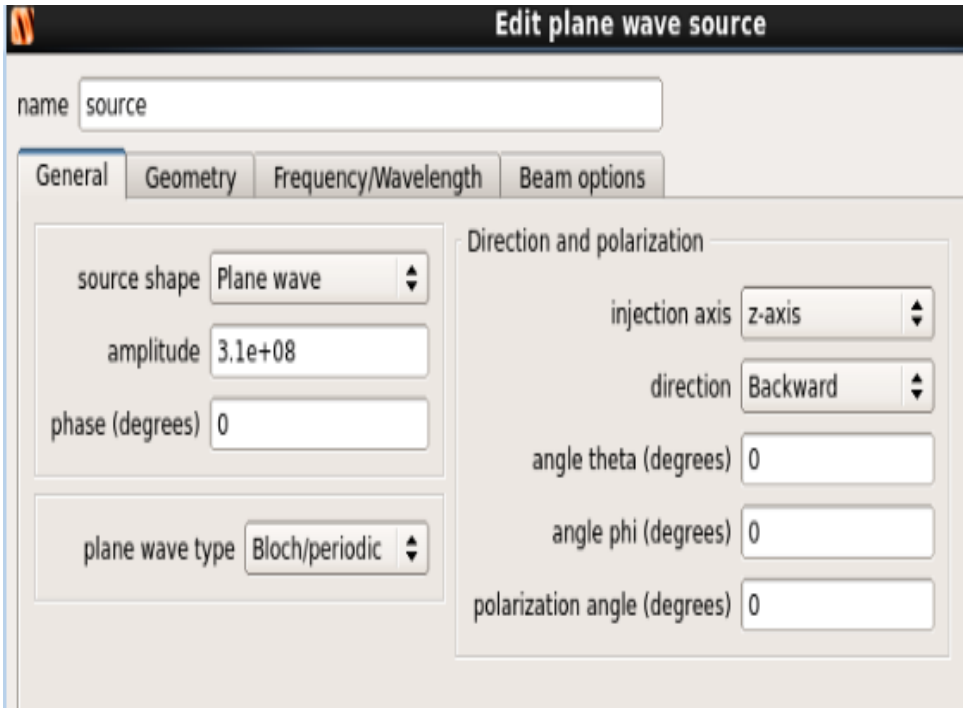

Figure A.1

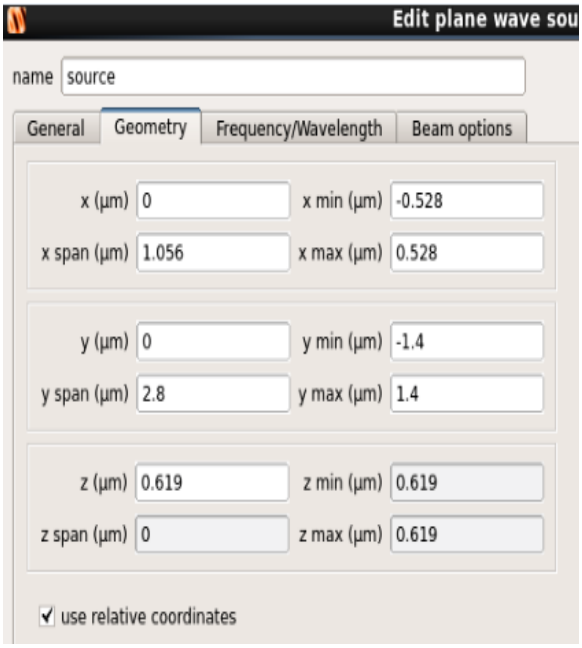

Figure A.2

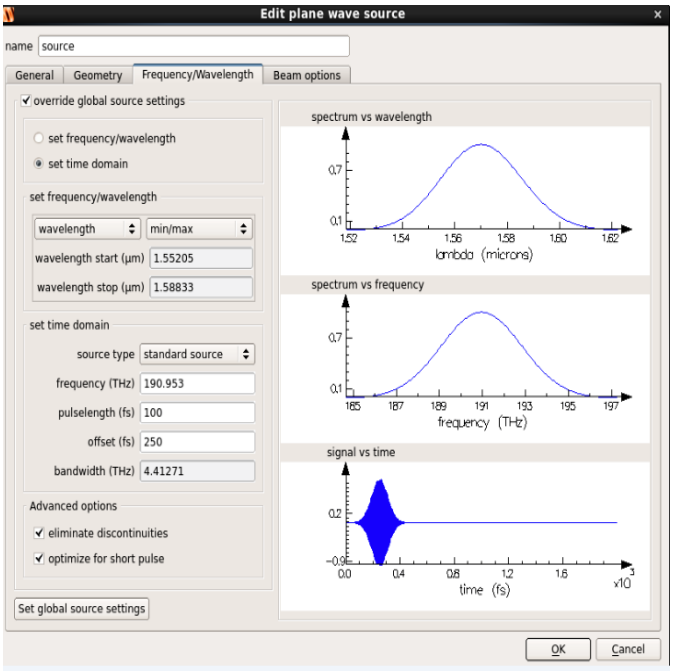

Figure A.3

II. Monitors

In this experiment, a monitor that records the transmitted electromagnetic fields collects our results. Frequency-domain field and power monitor was used to collect the field profile in the frequency domain from the simulation results. Note that the frequency-domain field and power was used because of its ability to snap to the nearest mesh cell when producing the results. Fig. (A.4 – A.6) shows the configuration of the monitor for this simulation. Calculating the average output power from the monitor was done using the pointing vector script. As shown below:

Poynting Vector code:

```
# disable CW norm
nonorm;

# get poynting vector from monitor.
Poynting = getresult("T_far_field_523","P");

# integrate real Pz to get power.  Assume this monitor is 2D, in the XY
plane
# This quantity will have units of Watts/Hz^2 due to the use of the
nonorm state
Trans = 0.5 * integrate(real(Poynting.Pz),1:2,Poynting.x,Poynting.y);

# package data into dataset
T = matrixdataset("T"); # initialize dataset
T.addparameter("lambda",c/Poynting.f,"f",Poynting.f); # add frequency
parameter
T.addattribute("T",Trans);  # add transmission attribute

# optionally, visualize data
visualize(T)
```

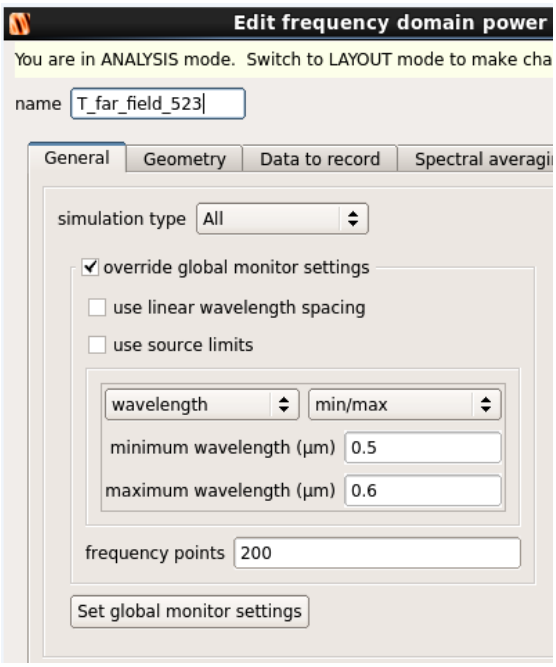

Figure A.4

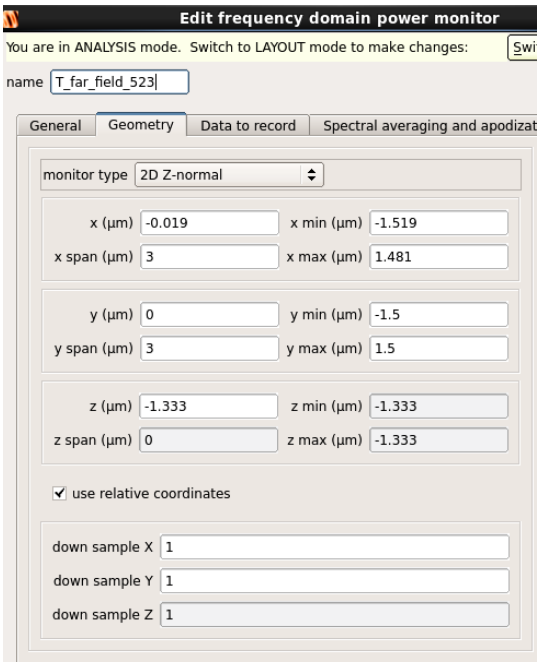

Figure A.5

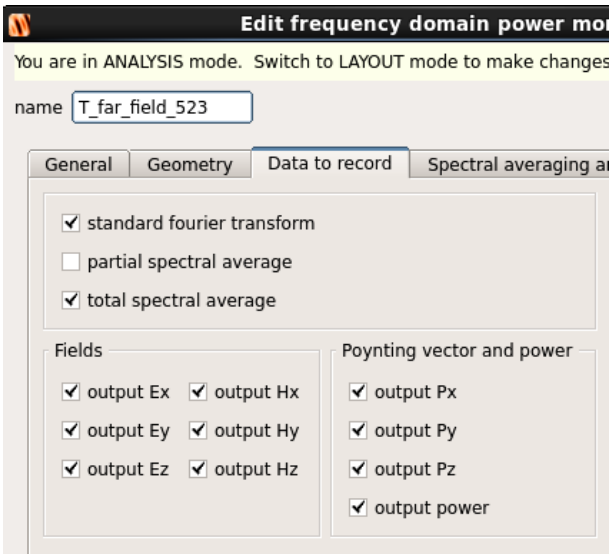

Figure A.6

III. Mesh

The mesh is used to define the position vectors x, y, z inside the defined boundary. The mesh is scaled in proportion to the size of our aperture. To find the correct mesh for a given structure, one would have to vary the mesh until it converges to a stable value. This is used to determine the accuracy of the simulation.

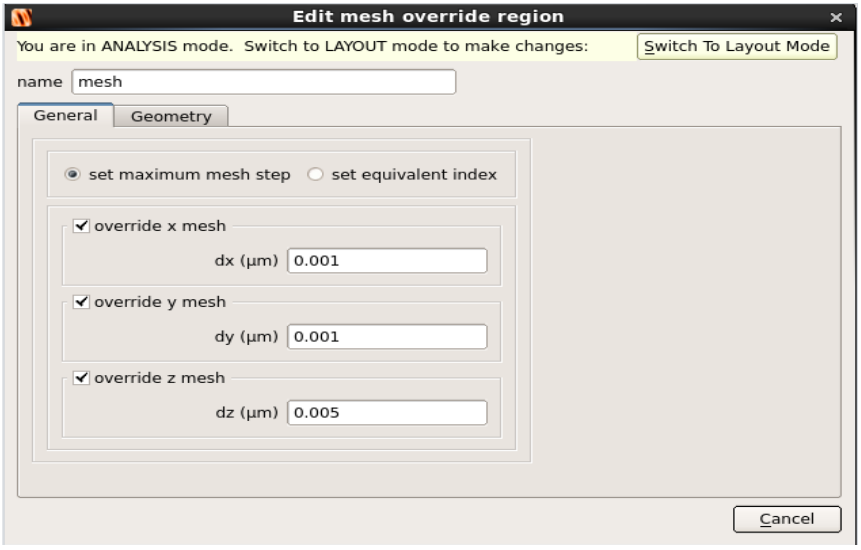

Figure A.7

IV. FDTD boundary conditions

The FDTD boundary condition also known as the simulation region is used to define a region over which the simulation is to be performed. The simulation region settings have some essential user-defined parameters that need to be configured as shown in Fig. (A.8 – A.11). Starting from the general tab where we define our simulation time and dimension, we move to configure the mesh settings using non-uniform mesh and set the mesh refinement. For this project, the boundary condition was set to periodic boundary condition because of the aperture in the design. Perfectly matched layer (PML) was also utilised to make sure that all the materials are matched and they absorb electromagnetic waves that is incident on them.

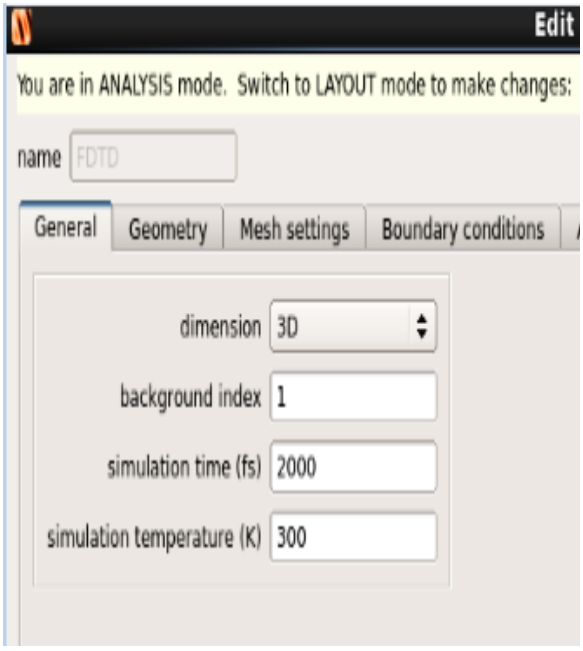

Figure A.8

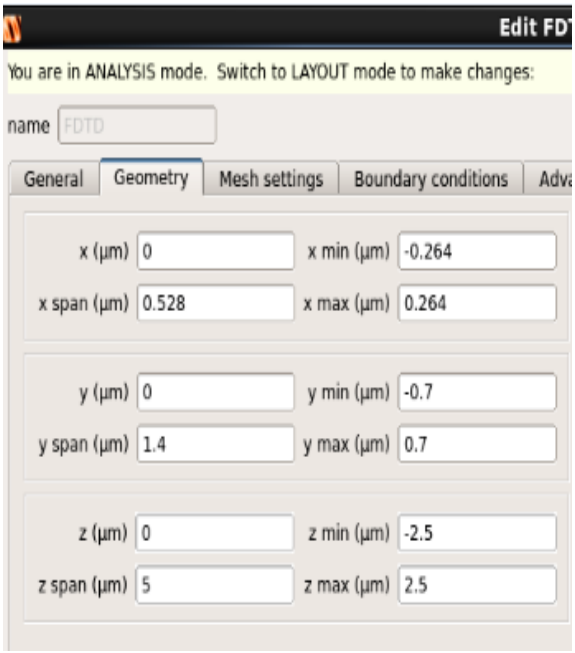

Figure A.9

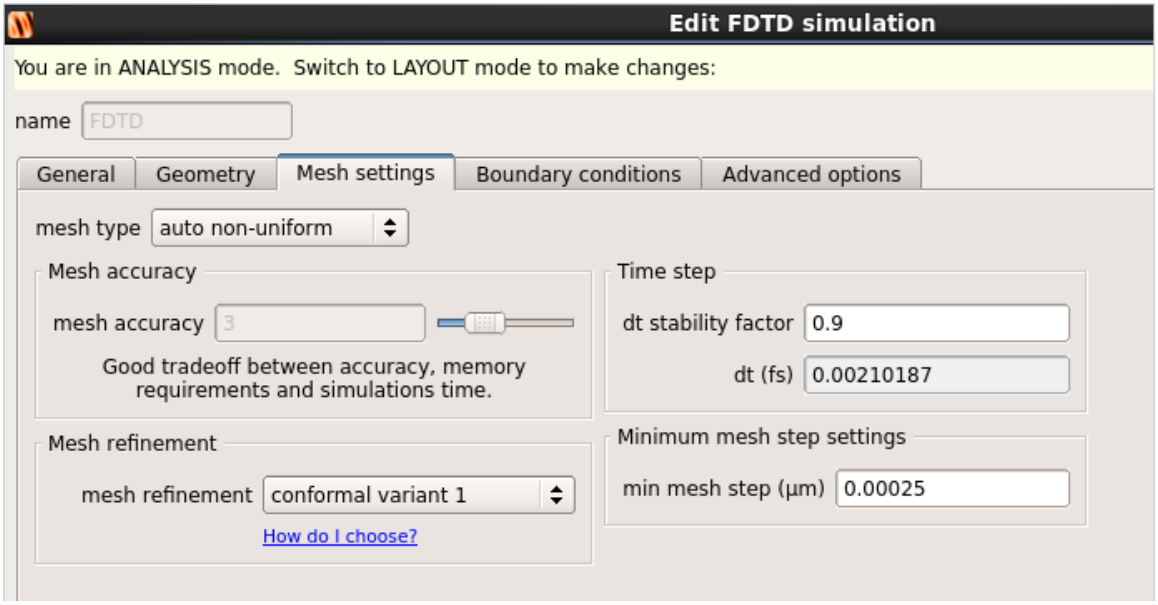

Figure A.10

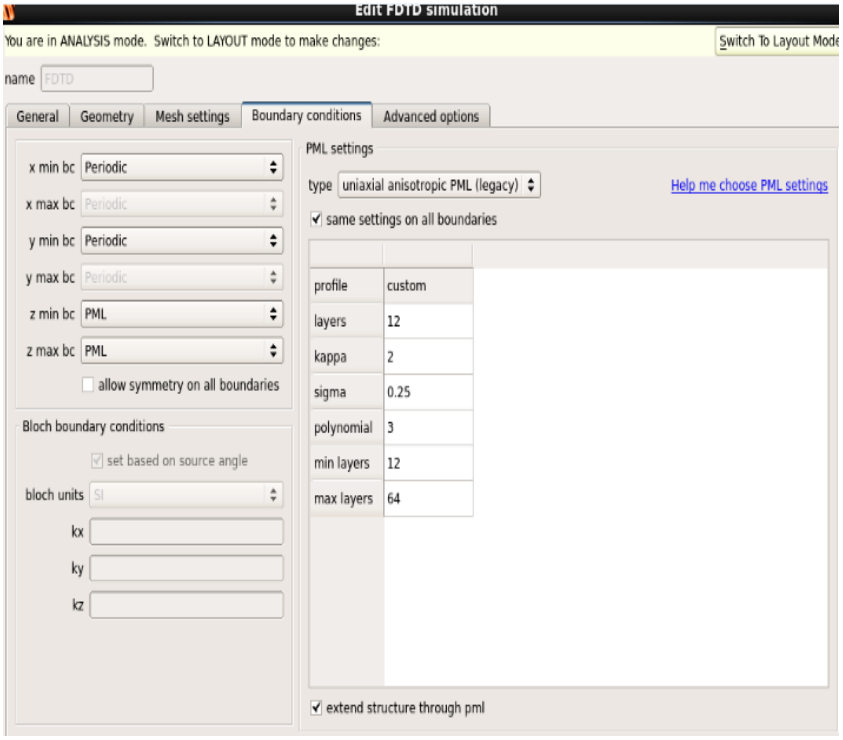

Figure A.11